FINAL REPORT

TO

OFFICE OF NAVAL RESEARCH

CONTRACT NO. N0001485K0437
N00014-85-K-0437

EFFECT OF TEMPERATURE ON THE CORROSION RESISTANCE OF NITROGEN BEARING AL6X AND 904L STAINLESS STEELS

BY

KIM GRETEL MARTIN

DEPARTMENT OF MATERIALS SCIENCE AND ENGINEERING
STATE UNIVERSITY OF NEW YORK
STONY BROOK, NY 11794-2275

SECURITY CLASSIFICATION OF THIS PAGE (When Data Entered)

REPORT DOCUMENTATION PAGE

READ INSTRUCTIONS BEFORE COMPLETING FORM

1. REPORT NUMBER	2. GOVT ACCESSION NO. / 3. RECIPIENT'S CATALOG NUMBER
4. TITLE (and Subtitle): Passivity Mechanisms in Stainless Steels: Mo-N Synergism	5. TYPE OF REPORT & PERIOD COVERED: Final Report / 6. PERFORMING ORG. REPORT NUMBER
7. AUTHOR(s): C.R. Clayton and Kim G. Martin	8. CONTRACT OR GRANT NUMBER(s): N 00014585K0437
9. PERFORMING ORGANIZATION NAME AND ADDRESS: State University of New York at Stony Brook, NY 11794	10. PROGRAM ELEMENT, PROJECT, TASK AREA & WORK UNIT NUMBERS
11. CONTROLLING OFFICE NAME AND ADDRESS	12. REPORT DATE: October 1988 / 13. NUMBER OF PAGES
14. MONITORING AGENCY NAME & ADDRESS(if different from Controlling Office)	15. SECURITY CLASS. (of this report) / 15a. DECLASSIFICATION/DOWNGRADING SCHEDULE

16. DISTRIBUTION STATEMENT (of this Report)

17. DISTRIBUTION STATEMENT (of the abstract entered in Block 20, if different from Report)

18. SUPPLEMENTARY NOTES

19. KEY WORDS (Continue on reverse side if necessary and identify by block number)

Passivity, XPS, Nitrogen, Stainless Steel

20. ABSTRACT (Continue on reverse side if necessary and identify by block number)

Potentiodynamic anodic polarization studies have shown that increasing the nitrogen content of AL6X from 0.04 wt.% to 0.19 wt% and that of 904L from 0.05 wt% to 0.20 wt% has dramatically improved the pitting resistance of these alloys. However, the greatest effect of nitrogen addition was noted with the AL6X stainless steels which had a 1.8 wt% greater molybdenum content. The contrast between the alloys became more distinct as the temperature of the electrolytes was raised. XPS analysis of the passive films formed on the AL6X alloys showed that both alloys produce a passive film more enriched

(see additional page)

DD FORM 1 JAN 73 1473 EDITION OF 1 NOV 65 IS OBSOLETE
S/N 0102-LF-014-6601

SECURITY CLASSIFICATION OF THIS PAGE (When Data Entered)

REPORT DOCUMENTATION PAGE
(#20 continued)

with chromium and molybdenum compared to the bulk composition, and that furtheringN alloying to 0.19 wt% the concentration of chromium and molybdenum in the passive film is further enriched. The aim of this study is to quantify the effect of nitrogen on passivation characteristics and pitting resistance as a function of temperature, and to elucidate a mechanism for the apparent nitrogen-molybdenum synergism.

EFFECT OF TEMPERATURE ON THE CORROSION RESISTANCE OF NITROGEN BEARING AL6X AND 904L STAINLESS STEELS

A Thesis presented

by

Kim Gretel Martin

to

The Graduate School

in Partial Fulfillment of the Requirements

for the Degree of

Master of Science

in

Materials Science and Engineering

State University of New York

at

Stony Brook

August 1988

Abstract of the Thesis

EFFECT OF TEMPERATURE ON THE CORROSION RESISTANCE OF NITROGEN BEARING AL6X AND 904L STAINLESS STEELS

by

Kim Gretel Martin

Master of Science

in

Materials Science and Engineering

State University of New York at Stony Brook

1988

Potentiodynamic anodic polarization studies have shown that increasing the nitrogen content of AL6X from 0.04 wt.% to 0.19 wt% and that of 904L from 0.05 wt% to 0.20 wt% has dramatically improved the pitting resistance of these alloys. However, the greatest effect of nitrogen addition was noted with the AL6X stainless steels which had a 1.8 wt% greater molybdenum content. The contrast between the alloys became more distinct as the temperature of the electrolytes was raised. XPS analysis of the passive films formed on the AL6X alloys showed that both alloys produce a passive film more enriched with chromium and molybdenum compared to the bulk composition, and that furthering N

alloying to 0.19 wt% the concentration of chromium and molybdenum in the passive film is further enriched. The aim of this study is to quantify the effect of nitrogen on passivation charateristics and pitting resistance as a function of temperature, and to elucidate a mechanism for the apparent nitrogen-molybdenum synergism.

TABLE OF CONTENTS

LIST OF FIGURES.....x

LIST OF TABLES.....xi

ACKNOWLEDGEMENTS.....xiii

I INTRODUCTION.....1

1.1 Literature Survey.....2

1.1.1 Nitrogen's Effect on Pitting Resistance and Passivity.....3

1.1.2 The Role of Molybdenum in Enhancing Passivity.....8

1.1.3 The Effect of Temperature on Corrosion Resistance of Mo-N Alloys...11

II EXPERIMENTAL PROCEDURES.....15

2.1 Introduction.....15

2.2 Materials and Preparation.....16

2.2.1 Materials.....16

2.2.2 Preparation of Stainless Steels.....16

2.3 Electrochemical Analysis.....16

2.3.1 Experimental Preparation.....16

2.3.2 Potentiodynamic Polarization.....17

2.3.3 Potentiostatic Polarization.....18

2.4 XPS Analysis.....19

2.4.1 Instrumentation and Operating Parameters.....19

2.4.2 Data Analysis.....20

III RESULTS.....21

3.1 Electrochemical Analysis.....21

3.1.1 Polarization Behavior of AL6X Alloys in 2N NaCl + 0.1M HCl.....21

3.1.2 Polarization Behavior of AL6X Alloys in 0.5M H_2SO_4.....22

3.1.3 Polarization Behavior of 904L Alloys in 2M NaCl + 0.1M HCl.....23

3.2 General Interpretation of the X-ray Photoelectron Spectra.....24

3.2.1 XPS Analysis of the Cr 2p 3/2 Spectra.....27

3.2.1.1 Ten second passivation at 0mV of AL6X alloys in 2M NaCl+0.1M HCl at 22C.....27

3.2.1.2 One hour passivation at 0mV of AL6X alloys in 2M NaCl+0.1M HCl at 22C.....28

3.2.1.3 Ten second passivation at 0mV of AL6X alloys in 2M NaCl+0.1M HCl at 45C.....29

3.2.1.4 One hour passivation at 0mV of AL6X alloys in 2M Nacl+0.1M HCl at 45C.....29

3.2.1.5 Ten second passivation at +400mV of AL6X alloys in 0.5M H_2SO_4 at 22C.....30

3.2.1.6 Ten second passivation at +400mV of AL6X alloys in 0.5M H_2SO_4 at 70C.....30

3.2.1.7 Ten second passivation at 0mV of 904L alloys in 2M NaCl+0.1M HCl at 22C.....31

3.2.2 XPS Analysis of Ni 2p 3/2 Spectra.....31

3.2.2.1 Ten second passivation at 0mV of AL6X alloys in 2M NaCl+0.1M HCl at 22C.....31

3.2.2.2 One hour passivation at 0mV of AL6X alloys in 2M NaCl+0.1M HCl at 22C.....32

3.2.2.3 Ten second passivation at 0mV of AL6X alloys in 2M NaCl+0.1M HCl at 45C.....32

3.2.2.4 One hour passivation at 0mV of AL6X alloys in 2M NaCl+0.1M HCl at 45C.....32

3.2.2.5 Ten second passivation at +400mV of AL6X alloys in 0.5M H_2SO_4 at 22C.....32

3.2.2.6 Ten second passivation at +400mV of AL6X alloys in 0.5M H_2SO_4 at 70C.....33

3.2.2.7 Ten second passivation at 0mV of AL6X alloys in 2M NaCl+0.1M HCl at 22C.....33

3.2.3 XPS Analysis of Mo 3d 5/2 Spectra.....33

3.2.3.1 Ten second passivation at 0mV of AL6X alloys in 2M NaCl+0.1M HCL at 22C.....33

3.2.3.2 One hour passivation at 0mV of AL6X alloys in 2M NaCl+0.1M HCl at 22C.....34

3.2.3.3 Ten second passivation at 0mV of AL6X alloys in 2M NaCl+0.1M HCl at 45C.....34

3.2.3.4 One hour passivation at 0mV of AL6X alloys in 2M NaCl+0.1M HCl at 45C.....35

3.2.3.5 Ten second passivation at +400mV of AL6X alloys in 0.5M H_2SO_4 at 22C.....35

3.2.3.6 Ten second passivation at +400mV of AL6X alloys in 0.5M H_2SO_4 at 70C.....36

3.2.3.7 Ten second passivation at 0mV of 904L alloys in 2M NaCl+0.1M HCl at 22C.....36

3.2.4 XPS Analysis of Fe 2p 3/2 Spectra.....37

3.2.4.1 Ten second passivation at 0mV of AL6X alloys in 2M NaCl+0.1M HCL at 22C.....37

3.2.4.2 One hour passivation at 0mV of AL6X alloys in 2M NaCl+0.1M HCl at 22C.....37

3.2.4.3 Ten second passivation at 0mV of AL6X alloys in 2M NaCl+0.1M HCl at 45C.....38

3.2.4.4 One hour passivation at 0mV of AL6X alloys in 2M NaCl+0.1M HCl at 45C.....38

3.2.4.5 Ten second passivation at +400mV of AL6X alloys in H_2SO_4 at 22C.....38

3.2.4.6 Ten second passivation at +400mV of AL6X alloys in H_2SO_4 at 70C.....39

3.2.4.7 Ten second passivation at 0mV of 904L alloys in 2M NaCl+0.1 HCl at 22C.....39

3.2.5 XPS Analysis of N 1s Spectra.....40

3.2.5.1 Ten second passivation at 0mV of AL6X alloys in 2M NaCl+0.1M HCl at 22C.....40

3.2.5.2 One hour passivation at 0mV of AL6X alloys in 2M NaCl+0.1M HCl at 22C.....40

3.2.5.3 Ten second passivation at 0mV of AL6X alloys in 2M NaCl+0.1M HCl at 45C.....41

3.2.5.4 One hour passivation at 0mV of AL6X alloys in 2M NaCl+0.1M HCl at 45C.....42

3.2.5.5 Ten second passivation at +400mV of AL6X alloys in 0.5M H_2SO_4 at 22C.....42

3.2.5.6 Ten second passivation at +400mV of AL6X alloys in 0.5M H_2SO_4 at 70C.....43

3.2.5.7 Ten second passivation at 0mV of 904L alloys in 2M NaCl+0.1M HCl at 22C.....43

3.3 Comparison of AL6X/N and 904L/N in 2M NaCl+0.1M HCl at 0mV and 22C.....44

3.4 Comparison of AL6X/N in 2M NaCl+0.1M HCl and 0.5M H_2SO_4.....46

3.4.1 At 22C.....46

3.4.2 At 45C in 2M NaCl+0.1M HCl and 70C in H_2SO_4.....47

IV DISCUSSION.....48

V CONCLUSIONS.....53

VI FUTURE WORK.....55

REFERENCES.....56

TABLES.....60

FIGURES.....81

LIST OF FIGURES

Figure 1 Comparison of the polarization curves of AL6X ss containing 0.04 wt% N in 2M NaCl + 0.1M HCl at 22, 37 and 40C.....82

Figure 2 Comparison of the polarization curves of AL6XN ss containing 0.19 wt% N in 2M NaCl + 0.1M HCl at 22, 37, and 40C....83

Figure 3 Comparison of the polarization curves of AL6X ss containing 0.04 wt% N in 2M NaCl + 0.1M HCl at 42 and 45C.....84

Figure 4 Comparison of the polarization curves of AL6XN ss containing 0.19 wt% N in 2M NaCl + 0.1M HCl at 42 and 45C.....85

Figure 5 Comparison of the polarization curves of AL6X ss containing 0.04 wt% N in 0.5M H_2SO_4 at 22 and 50C.....86

Figure 6 Comparison of the polarization curves of AL6XN ss containing 0.19 wt% N in 0.5M H_2SO_4 at 22 and 50C.....87

Figure 7 Comparison of the polarization curves of AL6X ss containing 0.04 wt% N in 0.5M H_2SO_4 at 75 and 85C.....88

Figure 8 Comparison of the polarization curves of AL6XN ss containing 0.19 wt% N in 0.5M H_2SO_4 at 75 and 85C.....89

Figure 9 Comparison of the polarization curves of 904L ss containing 0.05 wt% N in 2M NaCl + 0.1M HCl at 22 and 37C.....90

Figure 10 Comparison of the polarization curves of 904LN ss containing 0.20 wt% N in 2M NaCl + 0.1M HCl at 22 and 37C.....91

Figure 11 Comparison of the polarization curves of 904L ss containing 0.05 wt% N in 2M NaCl + 0.1M HCl at 40 and 45C.....92

Figure 12 Comparison of the polarization curves of 904LN ss containing 0.20 wt% N in 2M NaCl + 0.1M HCl ay 40 and 45C.....93

LIST OF TABLES

TABLE

1 Chemical Compositions of AL6X/N and 904L/N Alloys.....61

2 Electrochemical Characteristics of AL6X/N in 2M NaCl +0.1M HCl at various temperatures...62

3 Electrochemical Characteristics of AL6X/N in 0.5M H_2SO_4 at various temperatures.....63

4 Electrochemical Characteristics of 904L/N in 2M NaCl +0.1M HCl at various temperatures...64

5 Normalized Integrated Peak Areas for the main spectra obtained from the passive films formed on AL6X/N in 2M NaCl+0.1M HCl at 0mV (SCE) for 10 secs at 22C.....65

6 Normalized Integrated Peak Areas for the main spectra obtained from the passive films formed on AL6X/N in 2M NaCl+0.1M HCl at 0mV (SCE) for 1 hr at 22C.....66

7 Normalized Integrated Peak Areas for the main spectra obtained from the passive films formed on AL6X/N in 2M NaCl+0.1M HCl at 0mV (SCE) for 10 secs at 45C.....67

8 Normalized Integrated Peak Areas for the main spectra obtained from the passive films formed on AL6X/N in 2M NaCl+0.1M HCl at 0mV (SCE) for 1 hr at 45C.....68

9 Normalized Integrated Peak Areas for the main spectra obtained from the passive films formed on AL6X/N in 0.5M H_2SO_4 at +400mV (SCE) for 10 secs at 22C.....69

10 Normalized Integrated Peak Areas for the main spectra obtained from the passive films formed on AL6X/N in 0.5M H_2SO_4 at +400mV (SCE) for 10 secs at 70C.....70

11 Normalized Integrated Peak Areas for the main spectra obtained from the passive films formed on 904L/N in 2M NaCl+0.1M HCl at 0mV (SCE) for 10 secs at 22C.....71

12 Normalized Integrated Peak Area Ratios obtained from the passive films formed on AL6X/N in 2M NaCl+0.1M HCl at 0mV for 10s & 1hr at 22C....72

13 Normalized Integrated Peak Area Ratios obtained from the passive films formed on AL6X/N in 2M NaCl+0.1M HCl at 0mV for 10s & 1hr at 45C....73

14 Normalized Integrated Peak Area Ratios obtained from the passive films formed on AL6X/N in 0.5M H_2SO_4 at 400mV for 10s at 22C & 70C.....74

15 Normalized Integrated Peak Area Ratios obtained from the passive films formed on 904L/N in 2M NaCl+0.1M HCl at 0mV for 10s at 22C.....75

16 Atomic percentages of metals from underlying substrate obtained from the passive films formed on AL6X/N in 2M NaCl+0.1M HCl at 0mV for 10s and 1 hr at 22 and 45C.....76

17 Atomic percentages of metals from underlying substrate obtained from the passive films formed on AL6X/N in 0.5M H_2SO_4 at 400mV for 10s at 22 and 70C.....77

18 Atomic percentages of metals from underlying substrate obtained from the passive films formed on 904L/N in 2M NaCl+0.1M HCl at 0mV for 10s at 22C.....78

19 Peak Synthesis Parameters for N 1s and Mo 3p 3/2, and Fe 2p 3/2.....79

20 Peak Synthesis Parameters for Cr 2p 3/2 and Mo 3d.....80

I. INTRODUCTION:

There has been a marked increase in the demand and use of austenitic stainless steels as structural material, containing suitable levels of nitrogen in order to enhance strength characteristics [1-4]. There is an obvious economic advantage in using nitrogen in stainless steels, for nitrogen can replace or supplement the element nickel. Nitrogen which is an austenite stabilizer like nickel, has the benefit of being much less expensive and having thirty times the austenite forming potential of nickel [5]. Nitrogen has also been found to suppress the formation of secondary phases which are detrimental to corrosion resistance [6-9]. And nitrogen itself has been found to have a favorable effect on the improvement of corrosion resistance. Several studies have indicated that the addition of nitrogen to austenitic stainless steels can lead to improvements in passivation and pitting resistance [6-30]. It has also been repeatedly observed that the effect of nitrogen is greater in the presence of molybdenum, suggesting a possible synergism between molybdenum and nitrogen [6-8,11-15,21-30].

Temperature has been shown to be an important criterion for describing the onset of pitting corrosion in molybdenum containing austenitic stainless steels

[31-34]. Again, nitrogen proves to be a significant alloying element, for nitrogen considerably improves pitting resistance at elevated temperatures by raising the critical pitting temperatures of Fe-Ni-Cr-Mo alloys [6-7,12,17,24,29,31].

The mechanism by which nitrogen improves the passivity of austenitic stainless steels has not, as yet, been established. The purpose of this study has been to evaluate the influence of nitrogen alloying on corrosion behavior and passivation characteristics at both room temperature and elevated temperatures, and to establish a mechanism for the apparent synergism of molybdenum and nitrogen.

1.1 LITERATURE SURVEY:

The purpose of this section is to introduce previous studies that have investigated the passivation characteristics and effectiveness of the pitting resistance of austenitic stainless steels alloyed separately with molybdenum and nitrogen. And to examine the apparent synergistic effect when both elements are alloy constituents within the same steel. The effect of temperature on modifying electrochemical characteristics of the system has also been examined.

1.1.1 NITROGEN'S EFFECT ON PITTING RESISTANCE AND PASSIVITY:

Several studies have indicated that the addition of nitrogen to austenitic stainless steels can lead to improvements in passivation and pitting resistance [6-30]. By far, the greatest effect of N addition has been observed in molybdenum bearing stainless steels, suggesting a possible synergism between molybdenum and nitrogen [6-8,11-15,21-30].

Truman et. al. [15] studied the effect of N addition on pitting corrosion of a series of austenitic stainless steels. He observed that an increase in N content of a molybdenum free, 17Cr steel led to an increase in pitting potential, but improvements from increasing N were greater in the Cr-Mo steels, with a very marked improvement in the pitting potential observed in a 3% Mo series of steels.

Bandy and Van Rooyen [11,12] showed that still further enhancement of pitting resistance can be achieved by increasing the Mo content to 6%. Their experimental alloy, Alloy-30 with a nominal composition of 20Ni-24Cr-6Mo-0.44N wt% exhibited exceptional resistance to localized corrosion. A comparison of the polarization behavior of Alloys-30 and AL6X (with a composition of 25Ni-20Cr-6.3Mo-0.04N wt%) in 0.5M HCl +

3M NaCl at 50°C, showed that Alloy 30 was fully passive; by contrast, Alloy AL6X pitted immediately after passivation. The superior corrosion resistance of Alloy 30 compared to that of AL6X was considered to be due to the nitrogen in the former alloy.

Osozawa and Okato [10] noted that N has a greater effect in suppressing the growth of pits than Cr. They found that 0.2 wt% N was more effective in promoting pitting resistance than a 2% Cr addition to a 21Cr-22Ni-1.5Mo steel in 4% NaCl at 40°C.

Kearns [6] investigated the region of the active-passive transition for three AL6X alloys containing N in a very aggressive 4M HCl solution. He showed an increase of the critical pitting potential and a decrease of the current density as the N content of the AL6X alloy increased from 0.05 to 0.183 wt%.

Fukuzuka [30] has found that a 20Cr-22Ni-5Mo-0.2N alloy consistently had a lower current density than even a 20Cr-25Ni-6.5Mo alloy with only 0.02wt% N. This shows that there clearly is some kind of synergistic effect between the elements N and Mo.

However, the mechanism by which N improves the passivity and pitting resistance of austenitic stainless alloys has not been established, although a number of possible explanations have been put forward.

Results of several studies clearly demonstrate that the ammonium ion is the dominant nitrogen species in the bulk of the electrolyte after metal dissolution, even in potential ranges where nitrate ions would be expected to dominate on thermodynamic grounds [10,19]. After corrosion testing of N-containing steels in 20% ferric chloride solution, Osozawa and Okato [10] detected ammonium ions in the solution. This led them to suggest that when the N in the steel dissolves, it consumes protons in the pit via the reaction:

$$1/2N_2 + 4H^+ + 3e^- = NH_4^+$$

thus preventing further lowering of the pH in the pit due to metal hydrolysis and thus helping to passivate the pit before it exhibits steady growth.

Chigal et. al. [19] also observed the presence of NH_4^+ ions in their analysis of the solution after potentiostatic polarization in a 0.5%N alloyed steel in 1N H_2SO_4. They too, believe that the appearance of these ions in the surface layer of the solution must increase the pH of the near-electrode solution layer facilitating repassivation, which they proposed to be related to the established improvements in the passivation characteristics of nitrogen alloyed steels.

The possible role of N on passivity and the properties of the passive film have also been

discussed. Truman et. al. [19] were the first to put forward the suggestion that a metal nitride could coexist with and strengthen the lattice of a Cr-rich oxide film, and the formation of the nitride might be favored by an increased availability of atomic N at the surface of a steel with a high dissolved N content. Newman et. al. [22,23,25] investigated in this laboratory a 22-24Cr-20Ni-6Mo alloy with 0.04-0.5% N using XPS and AES analysis and found an enrichment of N at the metal-passive film interface after passivation in 0.5M H_2SO_4 and 2M NaCl + 0.5M HCl. They also reported that both Mo and N were enriched on the metal surface following selective dissolution preceeding repassivation. A barrier was therefore assumed to have been formed which inhibits further dissolution and allows nucleation of the passive film. When the film is formed it is initially enriched in Mo but finally attains its Mo depleted composition while N remains segregated at the metal-film interface.

In a later study, Clayton et. al. [21] reported that the formation of NH_3 and NH_4^+ at anodic potentials suggests a chemical rather than electrochemical mechanism of formation, since the formation of NH_4^+ would require a reduction process. The accumulation of CrN, by selective dissolution of Fe, however, would provide a condition in which N acts as an electron

acceptor. They proposed that the chemical breakdown of the Cr-N bond by a polar solvent (H_2O) would allow the Cr cation to be free for hydration and the N anions for protonation to NH_4^+. NH_4^+ would thus lower local acidity thereby aiding the stabilization of a film composed of Fe and Cr hydroxides. They proposed a secondary effect of NH_4^+ to be the formation of an ammonium sulfate salt layer, which would act as a temporary and not impermeable barrier between the metal and the solution thus inhibiting Cl- ion attack, during the initial stage of repassivation.

Newman has suggested two mechanisms for the N-Mo synergism, [22,27]. The first involves enrichment of both elements on the metal surface by selective dissolution during the active phase preceding repassivation. The second suggestion was that nitrogen atoms would enrich on the active surface and block mobile kink sites on the surface. This kink blockage would prevent, or delay to higher potentials, the attainment of extremely high current densities necessary for pit initiation.

1.1.2 THE ROLE OF MOLYBDENUM IN ENHANCING PASSIVITY:

It is known that the addition of Mo to austenitic stainless steels increases pitting resistance. The mechanism(s) by which the increased resistance is obtained is not well understood although many suggestions have been made as to the effect of alloyed molybdenum.

The fact molybdates can inhibit the corrosion of Fe-based alloys has led to mechanisms for molybdenums effect on the corrosion resistance of stainless steels based on molybdate formation. Ogawa et. al. [42] used AES and measurements of spontaneous passivation on Fe-Cr, Fe-Cr-Mo and Fe-Cr-Ni-Mo alloys and found that Mo retarded the breakdown of the passive film. In addition, Mo was detected in the passive films formed on Fe-25Cr-3Mo in Cl- containing solutions, and in those formed on Fe-19Cr-8Ni in the same solution with 0.01M Na_2MoO_4 added. They therefore proposed that metallic Mo dissolves as MoO_4^{2-} which absorbs at local active sites in the passive film and acts as an anodic inhibitor, reducing anodic dissolution and promoting the formation of a stable passive film.

Sugimoto and Sawada [30] reached similar conclusions after studying the passive region of 20Cr-25Ni-0-5Mo alloys in neutral NaCl solution with and

without Na_2MoO_4 additions. They found that MoO_4^{2-} ions act as an effective inhibitor against the pitting of austenitic stainless steels with and without Mo. Their XPS analyses showed Mo^{6+} to be present in the passive film regardless of whether Mo was introduced via dissolution of the metal or as MoO_4^{2-} addition to the electrolyte.

Other authors also suggest that Mo^{6+} in the passive film enhances passivity, however their models do not require molybdenum to be dissolved as molybdate before being adsorbed. Hashimoto et. al. [35,43] using XPS on ferritic Fe-30Cr-0-2Mo and Fe-19Cr-0-2Mo after passivation in 1M HCl, found the passive film formed above -200mV (SCE) to consist of hydrated Cr-oxyhydroxide. However, in the active state, in the potential region of -600 to -200 mV (SCE) Mo^{6+} was appreciably enriched on the surface. They suggested that Mo forms a surface film of Mo oxyhydroxide or Cr/Fe molybdate in the active state. This then decreases the activity of active surface sites on which it is otherwise difficult to form a stable passive film, and thereby promotes the formation of a stable Cr-oxyhydroxide passive film. Mo thus leads to a more uniform passive film and increases resistance to pitting corrosion by decreasing the activity of

micropores and promoting their repassivation before they develop pits.

Some authors believe that surface enrichment of metallic molybdenum enhances the passivation of alloys. Olefjord et. al.[40,41] have used XPS to investigate the surface films of Mo alloyed austenitic stainless steels after polarizing in the active and passive regions of the alloys in 0.1M HCl + 0.4M NaCl and 0.5M H_2SO_4. ESCA analyses showed that during active dissolution, the alloying elements Mo, Ni, Cr, are enriched on the surface in their metallic states. This enrichment is caused by preferential dissolution of Fe. It is suggested that this provokes passivation by lowering the dissolution rate in the active phase preceding passivation.

Newman [36,37] also favored a model where enrichment of elemental Mo played a greater role than its oxidized forms. He investigated the dissolution kinetics of scratched Fe-19Cr and Fe-19Cr-2.5Mo electrodes in 1M and 4M HCl and found that the inhibiting effect of Mo on active dissolution became apparent after dissolution corresponding to the removal of only 1.5-3 monolayers of alloy. This was explained by Mo dissolving slower than Fe and so accumulating in the elemental form at kink sites where primary dissolution occured.

Clayton et.al. [38,39] found evidence of a dual bipolar layer structure to the passive film on 19Cr-9Ni-0-2.5Mo using variable angle XPS studies. The bipolar film consists of a cation selective outer layer containing CrO_4^{2-} and MoO_4^{2-} and an intrinsically anion selective inner layer. The ion selective property of this duplex film is considered to be largely responsible for the development of a Cr_2O_3 barrier layer and resisting Cl- and OH- ingress.

1.1.3 THE EFFECT OF TEMPERATURE ON CORROSION RESISTANCE OF Mo-N ALLOYS:

The effect of temperature on pitting corrosion has been discussed in a limited number of publications. Previous data indicate that the character of the temperature dependence varies between different alloys.

Szklarska-Smialowska et. al. [33], contends that in both stages of the corrosion process, the initiation of pits and their development, are temperature dependent, but to a different degree. Since the chemisorption rate of chloride ions increases with increasing temperature, the breakdown of the passive layer at higher temperatures takes place sooner and at a lower potential. The number of pits formed at the same potential also increase with increasing

temperature, because at higher temperatures there are more sites susceptible to the nucleation of pits, since the limiting dissolution current increases with increasing temperature and as a result the initial current density in the pit at the higher temperature is larger than that observed at lower temperatures.

Brigham et. al. [31-32] found that the critical pitting temperature (CPT) at which pitting initiates, depends on the Mo content of the steel and the Cl- concentration of the solution used. Brigham noticed that although Mo plays the dominant beneficial role in improving pit initiation resistance, the beneficial effect of Mo addition decreases with increase in temperature. The authors suggested that a dependence on temperature rather than potential existed suggesting that there exists for each austenitic steel a critical pitting temperature below which the steel will not pit regardless of potential and exposure time, and that the average pitting behavior of all steels in the composition range 3 to 7.5% Mo can be described by the empirical equation:

$$CPT(^{o}C) = 10 + 7 \times \%Mo \qquad (1)$$

Brigham noted that this equation is only valid for pit nucleation on a flat surface, and that temperature values would be considerably reduced for the onset of

edge or crevice attack to occur.

Sugimoto and Sawada [34] studied the effect of temperature on anodic polarization curves of 20Cr-25Ni steels containing 1-5 wt% Mo in 0.1M NaCl. They also noticed the critical pitting temperature (which they defined as Tpit) became higher with increase in Mo content and they defined it as:

$$Tpit(^{o}C) = 5(Mo\%) + 20 \qquad (2)$$

The authors also investigated the temperature range in which MoO_4^{2-} ions showed an effective inhibition. They found Tpit of the 20Cr-25Ni Mo-free steel in 0.1M NaCl increased linearly with the MoO_4^{2-} concentration. They expressed this linear relation as:

$$Tpit(^{o}C) = 657.1\ (MoO_4^{2-}\ mol/l) - 32.28 \qquad (3)$$

Pitting of the steel in 0.1M NaCl below $70^{o}C$ was completely inhibited when the solution contained MoO_4^{2-} ions of more than 0.2M concentration.

J. Kolts et. al.[26] also defined an equation for the temperature at which pitting corrosion initiates. His corresponds to the Cr and Mo contents, i.e.:

$$T(^{o}C) = \%Cr + 2.4(\%Mo) \qquad (4)$$

The relationship has been found to be valid for austenitic Fe-Ni-Cr-Mo alloys, but may not apply to ferritic stainless steels or to alloys with substantial

amounts of other elements that effect pitting corrosion resistance such as W and N for example.

Janik-Czachor et. al. [17] were one of the first groups to investigate temperature effects on N-alloyed stainless steels. They noted that a modest temperature rise from 25°C to 40°C significantly lowers the resistance of a 18Cr-5Ni-10Mn steel containing 0.07-0.35% N in 0.1N H_2SO_4. For the 18Cr-5Ni-10Mn-0.35N steel the value of the potentiokinetic potential of pit nucleation was shifted about 250mV in the negative direction and that the induction time of pitting at 450mV was shortened from about 30 mins. at 25°C to 1 min. at 40°C.

J. Kearns [6] investigated type 317 stainless steels with three different N contents in a 0.1M HCl + 2M NaCl solution at 60°C, and showed that the critical pitting potential values increased with the N content.

The purpose of this paper has been to establish a mechanism(s) by which nitrogen improves the passivity of austenitic stainless steels, and to investigate the apparent synergistic effect of molybdenum and nitrogen. How temperature effects the corrosion resistant mechanism(s) has also been investigated.

II. EXPERIMENTAL PROCEDURES

2.1 INTRODUCTION

Electrochemical techniques and variable angle x-ray photoelectron spectroscopy, (XPS), have been used to determine the nature of the influence of N additions on passivity and corrosion inhibition of AL6X and 904L stainless steels as the solution temperature is raised. Anodic polarization scans were performed to study the variance of the electrochemical characteristics of the alloys in solutions of 2M NaCl + 0.1M HCl (pH= 0.7) and 0.5M H_2SO_4 (pH= 0.4) with increase in temperature of the electrolyte. XPS analysis of the high and low N alloys was performed following potentiostatic polarization in the above solutions at various solution temperatures. All XPS measurements were carried out at low (20^{o}) and high (50^{o}) photoelectron take-off angles, which were measured with respect to the plane of the sample, in order to observe the passive films and metal/film interfaces respectively. Compositional variations were also determined using XPS to examine the roles of nitrogen and the oxide films produced.

2.2 MATERIALS AND PREPARATION

2.2.1 MATERIALS

J. Kearns, of Allegheny Ludlum Steel Corporation, supplied the AL6X and 904LX stainless steel alloys along with their N alloy compositions, which are given in Table 1.

2.2.2 PREPARATION OF STAINLESS STEELS

The samples were cut into approximately 8x10x1 mm sized coupons and then ground with 240 and 600 grit silcon carbide paper. All samples were degreased by ultrasonic cleansing in proponal, washing in double distilled water and drying to air before being sealed in a preevacuated quartz tube and annealed at 1100^{o}C for three hours. This was followed by a water quench carried out by breaking the quartz tube under water. All the samples were again ground with 240 and 600 grit silicon carbide and then subsequently polished with 1 micron chromium oxide polish.

2.3 ELECTROCHEMICAL ANALYSIS

2.3.1 EXPERIMENTAL PREPARATION

After polishing, samples were degreased and cleaned in proponal and allowed to air dry before being mounted onto a plexiglass holder containing a copper wire for the electrical connection to the

potentiostat. Five-minute epoxy was then used to seal the edges and sides of the sample so that only the polished surface was exposed to the electrolyte. The epoxy was allowed to cure for at least 48 hours prior to any sample use.

The electrolytes used were prepared from reagent grade chemicals, where solid chemicals were weighed to the nearest 0.5 mg and liquids to the nearest 0.5 ml. All solutes were diluted in double distilled water and measurements of solution pH were of +0.1 accuracy.

2.3.2 POTENTIODYNAMIC POLARIZATION

Cyclic polarizations were performed in a conventional Greene cell using either 2M NaCl + 0.1M HCl (pH= 0.7) or 0.5M H_2SO_4 (pH= 0.4) which were deaerated by purging with pre-purified argon for 2 hours. A positive pressure of argon was maintained in the cell throughout the duration of the experiment and a magnetic, teflon stir bar provided constant circulation of the solution. When required, the Greene cell was immersed in a constant temperature water-bath to regulate the temperature of the electrolyte used. All potentials were measured against a saturated calomel electrode (SCE). Specimens were cathodically treated at -550 mV for 15 minutes to reduce the polished-formed film. The specimens were then

potentiodynamically polarized in the anodic direction at 0.3 mV/s at either room temperature (22°C) or an elevated temperature, up to 45°C in the chloride solution, or up to 85°C in the sulfuric solution, to obtain polarization curves. To indicate whether pitting of the sample surface had occured in the chloride solution, the direction of the polarization scan was reversed after breakdown of the passive film was indicated. The onset of breakdown or pitting was indicated by a sharp increase in the current density.

2.3.3 POTENTIOSTATIC POLARIZATION

Potentiostatic polarization experiments were used to prepare anodic films for XPS analysis. A similar experimental set-up to that of the potentiodynamic polarizations was used, except, after cathodically pre-treating for 15 minutes, the specimens were pulsed to a specified potential and maintained there for a specified time to generate anodic films. Following the passivation treatment, the samples were removed from the cell, washed with deaerated, double distilled water, and dried with a stream of argon. After careful removal of the epoxy, the samples were mounted on a degreased copper sample holder by way of double stick tape. Electrical contact was obtained by brushing conductive silver paint between the sides of

the sample and the copper sample holder, which was then mounted onto the XPS probe. The entire operation was carried out in a pre-purified argon purged glove box. The samples were then transferred under argon to the specimen preparation chamber of the electron spectrometer which was purged with pre-purified argon. The argon was used to prevent gross atmospheric oxidation of the samples.

2.4 XPS ANALYSIS

2.4.1 INSTRUMENTATION AND OPERATING PARAMETERS

All XPS measurements were performed with a V.G. Scientific ESCA 3 Mark II controlled by a V.G. Scientific Data System 1000. The system was equipped with a hemispherical analyser which was operated in the constant analyzer energy (CAE) mode. An Al $K_{1,2}$ (1486.6 eV) source was used for XPS and operated at 400 watts. The base pressure was approximately 1.5×10^{-9} torr. Narrow elemental scans of 25 eV width were obtained with the spectrometer's analyser set at 20 eV pass energy. All XPS measurements were carried out at high (50°) and low (20°) photoelectron take-off angles, which were measured with respect to the plane of the sample, in order to observe the inner and outer layers of the films respectively [45]. For reference the

binding energy of the Au 4f 7/2 line was taken as 83.8 eV and was found to have a FWHM of 1.4 eV under the experimental conditions. The XPS spectra were corrected for charge shifting by taking the carbon 1s spectrum at 284.6 eV.

2.4.2 DATA ANALYSIS

All data were smoothed, utilizing a 15 point quadratic/cubic least squares program following the method developed by Savitsky and Golay [46] which was modified by Sherwood [47] to cover the truncation errors at the ends of the spectra. Since the Cr $2p_{1/2}$ peak produces an Al K $_{3,4}$ satellite on the high binding energy side of the Cr $2p_{3/2}$ peak, a satellite subtraction program dependent on the analyser pass energy was used to eliminate the Cr $2p_{1/2}$ satellite. For peak synthesis, fitting parameters included the peak's position, height, full width half maximum, Gaussian/Lorentzian ratio, and tail characteristics which are height, slope, and exponential to linear tail mix [47]. The parameters used came from this research group's work on standards and supplemented by those given in the literature.

III. RESULTS:

3.1 ELECTROCHEMICAL ANALYSIS:

3.1.1 POLARIZATION BEHAVIOR OF AL6X ALLOYS IN 2M NaCl + 0.1M HCl:

The polarization behavior of AL6X alloys in 2M NaCl + 0.1M HCl (pH 0.7) at various solution temperatures is presented in Figures 1-4. The pertinent electrochemical features of the samples are given in Table 2. It is evident from Figures 1-4 and Table 2 that an increase in N content has a significant effect on pitting resistance as the temperature of the electrolyte is raised. It is observed that the higher N steel consistently exhibited higher breakdown potentials than the low N steel as the temperature was raised. Below 40^{o}C, both alloys have extensive passive regions Figures 1-4 shows that the high N-alloy polarization curves are consistently more stable than that of the low N-alloy. At 40^{o}C only AL6XN was able to go transpassive, and beyond that temperature, both alloys pitted. The addition of N also resulted in a slight decrease of the passive current density throughout the temperature range. An interesting phenomenon is to be noted. A comparison of the critical current densities of the two alloys shows that

at room temperature they have similar critical current densities. As the temperature is raised to 37°C, the critical current density of the low N alloy is almost doubled that of the high N alloy. When the temperature is further raised to 40°C, the low N alloy again has a greater critical current density compared to the high N alloy. This time of approximately 15 uA/cm^2. However, when the temperature is then raised to 42°C, there is a turn-about. The high N alloy now has a critical current density that is twice as great as that of the low N alloy. A further increase in temperature to 45°C still gives the high N alloy a greater critical current density over the low N alloy, but only by about one third.

3.1.2 POLARIZATION BEHAVIOR OF AL6X ALLOYS IN 0.5M H_2SO_4:

Polarization traces of the AL6X alloys in 0.5M H_2SO_4 (pH 0.4) at various solution temperatures are shown in Figures 5-8. Their salient electrochemical characteristics are given on Table 3. Both alloys have extensive passive ranges for all test temperatures up to 85°C. For exposure in 0.5M H_2SO_4, the beneficial influence of N-alloying can best be seen by the critical current density values.

The high N alloy consistently shows lower critical current density values compared to the low N alloy. At 85°C the low N alloy has a critical current density which is more than 5 times greater than that of the high N alloy.

It can be seen from Figures 1-8 and Tables 1-2, that AL6X and AL6XN show better passivity characteristics at elevated temperatures in the sulfuric solution than in the chloride solution, even though the sulfuric solution is slightly more acidic with a pH of 0.4. This suggests that perhaps both SO_4^{2-} and N are responsible for the increased pitting resistance in this solution, and therefore requires further enquiry.

3.1.3 POLARIZATION BEHAVIOR OF 904L ALLOYS IN 2M NaCl + 0.1M HCl:

The polarization curves for the 904L and 904LN alloys in 2M NaCl + 0.1M HCl are presented in Figures 9-12. The pertinent electrochemical characteristics are given in Table 4. The main difference between the 904L alloys and the AL6X alloys, is that the 904Ls have 1.8 wt% less molybdenum than the AL6X alloys. It can be seen from Table 2 and Table 4 that the passivation potential values decrease and the pitting potential values increase as the amount of Mo is increased. The

combination of these two changes represents an expansion in the range of potentials where the alloys are passive in acidic solutions. It can be seen that an addition of 1.8 wt% Mo to both the low and high N alloys has a significant, beneficial influence on the critical curent density, and therefore, on the active dissolution. Even the low-N AL6X alloy has better passivation characteristics than that of the high-N 904L alloy. This shows, that there is a very strong combined or synergistic effect between the elements molybdenum and nitrogen, and the effect is heightened with an increase in Mo content in the 2M NaCl + 0.1M HCl solution.

3.2 GENERAL INTERPRETATION OF THE X-RAY PHOTOELECTRON SPECTRA:

To aid in the comparison of the 20^{o} and 50^{o} spectra obtained from the passive films, the peak area intensities are presented in Tables [5-15]. The peak areas were normalized to the total peak area of the oxidized metal signals. This semiquantitative analysis provides a convenient guide to the relative abundance of the various species in the inner and outer regions of the passive films. In order to determine whether

metallic components in the steels were enriched or depleted relative to the bulk following anodic polarisation treatments, the peak area intensities of the pure metallic components were converted to atomic percentages for comparison with the bulk atomic percentages of the alloys. These are presented in Tables [16-18] for each of the experiments.

Narrow scan spectra of N1s, Cr2p, Mo3d, O1s, Fe2p, Ni2p and C12p or S2p were analyzed for each of the experiments. The binding energies for all the components are given in Tables [19-20].

Cr 2p 3/2 Spectra: Five components were found in each case corresponding to the following species: (i) metallic Cr from the substrate, (ii) Cr^{3+} corresponding to Cr_2O_3, (iii) Cr^{3+} corresponding to $Cr(OH)_3$, (iv) Cr^{6+} corresponding to CrO_3 and (v) Cr^{6+} corresponding to CrO_4^{2-}. This is consistent with other studies reported by this group [21,25].

Ni 2p 3/2 Spectra: Only metallic Ni was observed for each of the samples at all temperatures and passivation times. No evidence of oxidized Ni could be found.

Cl 2p Spectra: For experiments run in the chloride solution, the Cl 2p spectra showed an increase in the Cl- content at the low take-off angle for each of the treatments.

Mo 3d 5/2 Spectra: The Mo spectra exhibited three components: Metallic Mo, Mo^{4+} which is assumed to be a hydrated form of $MoO(OH)_2$, and Mo^{6+} which is identified as MoO_4^{2-}.

O 1s Spectra: Three components were clearly discernable; (i) O^{2-} (ii) OH- and (iii) adsorbed H_2O; in sulfuric solution SO_4^{2-} was also observed. All were seen at both 20° and 50° take-off angles. The OH^- species, H_2O, and SO_4^{2-} when sulfuric solution was used, were in great abundance at the 20° spectral analysis compared to the O^{2-} species. This indicates an enrichment of these species at the outer most part of the film. O^{2-} was found in greatest abundance at the metal-film interface.

N 1s Spectra: Three distinct N species were observed; (i) a nitride, (ii) NH_3 and (iii) NH_4^+. All were seen at both 20° and 50° take-ofr angles. The 20° analysis infers that NH_4^+ is enriched at the outer most part of the film, while NH_3 is throughout the main body of the film.

Fe 2p 3/2 Spectra: Three components to the multiplet were found in each case corresponding to: (i) metallic Fe from the substrate, (ii) Fe^{2+} and (iii) Fe^{3+}.

3.2.1 XPS ANALYSIS OF THE Cr 2p 3/2 SPECTRA (TABLES 5-18):

3.2.1.1 Ten second passivation at 0mV of AL6X alloys in 2M NaCl + 0.1M HCl at 22C:

The underlying substrate composition showed little variation in Cr with increase in the N content. Both alloys were enriched with metallic Cr by 26% compared to the bulk composition. AL6XN has a stronger Cr^{3+} spectra at 50^{o} compared to that of AL6X. However, the ratio of the peak areas for Cr_2O_3 and $Cr(OH)_3$ is only slightly higher for AL6XN.

Compared to the other alloying elements, both alloys have a surface enrichment of metallic Cr; AL6XN is enriched by 30% and AL6X by 21%. In the 20^{o} analysis, AL6XN has a greater content of the Cr^{3+} species, Cr_2O_3 and $Cr(OH)_3$, in its outer film than AL6X. However, the ratio of the peak areas of Cr_2O_3 and $Cr(OH)_3$ is slightly greater for the low N alloy.

3.2.1.2 One hour passivation at 0mV of AL6X alloys in 2M NaCl + 0.1M HCl at 22C:

The underlying substrate composition of the high N alloy contained 12% more Cr compared to the low N alloy. The underlying substrate for AL6XN showed an approxiate 40% increase of Cr compared to the bulk composition, whereas AL6X showed a 13% increase compared to the bulk. The 50^{o} spectra analysis shows that AL6XN, in comparison to AL6X, has a greater amount of Cr_2O_3 and Cr^{6+} species at the metal-film interface, but AL6X has more $Cr(OH)_3$ at the metal-film interface. As a result, the peak area ratio of Cr_2O_3 to CrO_3 is larger for the high N alloy. Refering to Tables 6 and 7, it can be seen that the amount of metallic Cr in the underlying substrate of AL6X decreases with increasing passivation time. Whereas, the amount of Cr in the substrate of AL6XN shows no variation with time of passivation.

The 20^{o} spectral analysis shows that the ratio of the peak areas of Cr_2O_3 to $Cr(OH)_3$ is slightly greater for the high N alloy. This correlates well with the fact that there is more MoO_4^{2-} in the film of AL6XN, and therefore the film experiences enhancement of MoO_4^{2-} induced deprotonation. AL6X shows a decrease in the amount of $Cr(OH)_3$ with passivation time.

3.2.1.3 Ten second passivation at 0mV of AL6X alloys in 2M NaCl + 0.1M HCl at 45C:

The 50^{o} spectral analysis shows that the underlying substrates of both alloys were enriched by 26% compared to the bulk composition. The 50^{o} spectra analysis shows there is relatively no difference in the amount of Cr^{3+} at the metal-film interface for the two alloys. In fact, they have the same ratio for the peak areas of Cr_2O_3 to $Cr(OH)_3$. The analysis shows, however, that the high N alloy has a greater relative amount of Cr^{6+} at this interface.

The 20^{o} spectral analysis shows that the ratio of the peak areas of Cr_2O_3 to $Cr(OH)_3$ is slightly greater for the low N alloy.

3.2.1.4 One hour passivation at 0mV of AL6X alloys in 2M NaCl + 0.1M HCl at 45C:

The underlying substrate for both alloys shows an approximate 20% increase of Cr compared to the bulk composition. The 50^{o} spectral analysis shows that both alloys have relatively the same amount of Cr^{3+} and Cr^{6+} at their metal-film interface. Both alloys have an enrichment of Cr in their films of approximately 30%. The ratio for the peak areas of the Cr^{3+} species is slightly greater for the high N alloy.

3.2.1.5 Ten second passivation at +400mV of AL6X alloys in 0.5M H_2SO_4 at 22C:

The 50^{o} spectral analysis shows that both alloy substrates are enriched by an approximate 36% compared to the bulk composition. The relative amounts of both Cr^{3+} species is the same for the two alloys and hence, their peak area ratios are the same. Compared with AL6X, AL6XN has a slightly greater amount of the Cr^{6+} species at the metal-film interface.

Both alloys have similar surface enrichments of 36% of metallic Cr. Here at the film-solution interface, the peak area ratios for Cr_2O_3 and $Cr(OH)_3$ are again the same for the two alloys.

3.2.1.6 Ten second passivation at +400mV for AL6X alloys in 0.5M H_2SO_4 at 70C:

The underlying substrate of both alloys shows an approximate 36% enrichment of metallic Cr compared to the bulk composition. At the metal-film interface, AL6XN has a Cr_2O_3 to CrO_3 ratio which is 2.7 times greater than that of AL6X. This is due to the amount of Cr_2O_3 decreasing by a factor of three as the temperature increases from $22^{o}C$ to $70^{o}C$ for AL6X.

The 20^{o} spectral analysis shows the surface of both alloys is enriched with metallic Cr. AL6XN is enriched

by 18% and AL6X by 12%. Both alloys have the same Cr_2O_3 to $Cr(OH)_3$ peak area ratios.

3.2.1.7 Ten second passivation at 0mV of 904L alloys in 2M NaCl + 0.1M HCl at 22C:

The 50° spectra analysis shows that the underlying substrates of both alloys are enriched with metallic Cr by 23% compared to the bulk composition. AL6XN has a ratio of the peak areas for Cr_2O_3 and CrO_3 which is 1.5 times as great as that for AL6X.

The 20° spectral analysis shows a surface enrichment of metallic Cr of 10% for both alloys. AL6XN has a ratio of the peak areas of Cr_2O_3 to $Cr(OH)_3$ which is twice as great as that for AL6X.

3.2.2 XPS ANALYSIS OF Ni 2p 3/2 SPECTRA (TABLES 5-18):

3.2.2.1 Ten second passivation at 0mV of AL6X alloys in 2M NaCl + 0.1M HCl at 22C:

The 50° spectral analysis shows that Ni was found to be depleted in the substrate by at least 50% for both alloys.

3.2.2.2 One hour passivation at 0mV of AL6X alloys in 2M NaCl + 0.1M HCl at 22C:

At 50° the underlying substrate composition of the high N alloy shows there is about 35% less Ni compared to the low N alloy. Ni is found to be depleted in the substrate of the high N alloy by at least 50% compared to the bulk composition.

3.2.2.3 Ten second passivation at 0mV of AL6X alloys in 2M NaCl + 0.1M HCl at 45C:

Nickel was found to be depleted in the substrate by at least 50% for both alloys.

3.2.2.4 One hour passivation at 0mV of AL6X alloys in 2M NaCl + 0.1M HCl at 45C:

Both alloys have a Ni depletion of the substrate by 34% compared to the bulk.

3.2.2.5 Ten second passivation at +400mV of AL6X alloys in 0.5M H_2SO_4 at 22C:

Both alloys are similarly depleted of metallic Ni by 50% in their underlying substrate compared to the bulk composition.

3.2.2.6 Ten second passivation at +400mV of AL6X alloys in 0.5M H_2SO_4 at 70C:

Ni was found to be depleted in the substrate by 50% compared to the bulk composition for both alloys.

3.2.2.7 Ten second passivation at 0mV of 904L alloys in 2M NaCl + 0.1M HCl at 22C:

Both alloys are depleted of Ni in their substrates compared to the bulk composition. The low N alloy is depleted by approximately 20% and the high N alloy by 34%.

3.2.3 XPS ANALYSIS OF Mo 3d 5/2 SPECTRA (TABLES 5-18):

3.2.3.1 Ten second passivation at 0mV of AL6X alloys in 2M NaCl + 0.1M HCl at 22C:

The 50^{o} spectra analysis shows that the underlying substrates of both alloys are enriched with metallic Mo by at least 50% compared to the bulk composition.

The 20^{o} spectra reveals a surface enrichment of metallic Mo by 33% for AL6X and 46% for AL6XN. Also, MoO_4^{2-} is enhanced at this angle and hence is apparently nearer to the film-solution interface. $MoO(OH)_2$ is distributed evenly throughout the film according to both angular analysis.

3.2.3.2 One hour passivation at 0mV for AL6X alloys in 2M NaCl + 0.1M HCl at 22C:

Metallic Mo is found to be enriched in the substrate of the high N alloy by about 50% compared to the bulk composition and by 32% for the low N alloy. To be noted, is the fact that the low N alloy generates 41% more metallic Mo at its metal-film interface after 10 seconds than after 1 hour of passivation. The high N alloy showed little variation of Mo content with time.

According to the 20^{o} spectral analysis, MoO_4^{2-} is enhanced at this angle and therefore is nearer to the film-solution interface. $MoO(OH)_2$ is also slightly more enhanced at this angle and one would infer that $MoO(OH)_2$ is also more abundant at the film-solution interface.

3.2.3.3 Ten second passivation at 0mV for AL6X alloys in 2M NaCl + 0.1M HCl at 45C:

The 50^{o} spectral analysis shows that both alloys are again enriched with metallic Mo by at least 50% compared to the bulk composition. AL6X shows the Mo^{4+} species, $MoO(OH)_2$, to be more abundant at this angle, hence, MoO_2 closer to the metal-film interface.

The 20^{o} spectral analysis reveals that both alloys have an enrichment of MoO_4^{2-} at this angle, suggesting that the species is nearer to the film-solution interface. AL6XN also shows a greater amount of the Mo^{4+} species in this region, which predicts MoO_2 to be at the outer regions of the film.

3.2.3.4 One hour passivation at 0mV of AL6X alloys in 2M NaCl + 0.1M HCl at 45C:

According to the 50^{o} spectra, the underlying substrates of both alloys are enriched with metallic Mo by approximately 38% compared to the bulk compostion.

The 20^{o} spectra analysis reveals that there is a surface enrichment of the metallic species for both alloys of approximately 50%. MoO_4^{2-} is enhanced at this angle for both alloy and hence is apparently nearer to the film-solution interface. $MoO(OH)_2$ seems to be evenly distributed thoughout the film for both alloys.

3.2.3.5 Ten second passivation at +400mV of AL6X alloys in 0.5M H_2SO_4 at 22C:

The 50^{o} spectral analysis shows a substrate enrichment of metallic Mo by 47% for AL6X and by 43% for AL6XN.

MoO_4^{2-} is evenly distributed throughout the film of AL6X. AL6XN, however, shows the 6+ species to be more enhanced in the 20^{o} analysis and hence nearer to the film-solution interface. MoO_2 seems to be located nearer to the metal-film interface for both alloys.

3.2.3.6 Ten second passivation at +400mV of AL6X alloys in in 0.5M H_2SO_4 at 70C:

The underlying substrates of both alloys have an enrichment of metallic Mo of approximately 50%.

The 20^{o} spectra analysis shows that MoO_4^{2-} is more enhanced at this angle for the low N alloy and therefore is apparently nearer to the film-solution interface. The 6+ species is more evenly distributed throughout the film of the high N species. Likewise, MoO_2 is evenly distributed throughout the film of both alloys.

3.2.3.7 Ten second passivation at 0mV for 904L alloys in 2M NaCl + 0.1M HCl at 22C:

The 50^{o} spectra analysis reveals that both alloys have underlying substrates which are enriched with metallic Mo compared to the bulk composition. The high N alloy is enriched by 60% and the low N alloy by 43%. The spectra of AL6XN also shows an enhancement of MoO_2

at this angle indicating its location to be at the inner regions of the film. For AL6X, both MoO_4^{2-} and MoO_2 are approximately evenly distributed throughout its film.

The 20° spectra analysis shows an enhancement of MoO_4^{2-} for the high N alloy, indicating its location to be in the outer regions of the film.

3.2.4 XPS ANALYSIS OF Fe 2p 3/2 SPECTRA (TABLES 5-18):

3.2.4.1 Ten second passivation at 0mV of AL6X alloys in 2M NaCl + 0.1M HCl at 22C:

The 50° spectra analysis showed that Fe is neither enriched nor depleted in the substrates of the two alloys. However, both alloys showed a little stronger contribution in the spectra from Fe^{3+} at 50° i.e., Fe^{3+} is enriched relative to Fe^{2+} at the metal-film interface.

3.2.4.2 One hour passivation at 0mV of AL6X alloys in 2M NaCl + 0.1M HCl at 22C:

Metallic Fe is neither enriched nor depleted in the substrates of the two alloys. However, both alloys showed a stronger contribution in the spectra from both Fe^{2+} and Fe^{3+} at 50°, i.e., they are apparently deeper within the film, closer to the metal-film interface.

3.2.4.3 Ten second passivation at 0mV of AL6X alloys in 2M NaCl + 0.1M HCl at 45C:

The spectra analysis reveals that Fe is neither enriched nor depleted in the substrates of the two alloys. At the elevated temperature, the composition of Fe^{2+} and Fe^{3+} ions are more evenly distributed throughout the film.

3.2.4.4 One hour passivation at 0mV of AL6X alloys in 2M NaCl + 0.1M HCl at 45C:

Again, Fe is neither enriched nor depleted in the substrates of the two alloys. Also, compared to the 22C experiment, the composition of Fe^{2+} and Fe^{3+} ions are more evenly distributed throughout the film.

3.2.4.5 Ten second passivation at +400mV of AL6X alloys in 0.5M H_2SO_4 at 22C:

Both alloys are neither enriched nor depleted in their underlying substrates compared to the bulk composition. For both alloys, Fe^{3+} is slightly enriched relative to Fe^{2+} at the metal-film interface.

3.2.4.6 Ten second passivation at +400mV of AL6X alloys in 0.5M H_2SO_4 at 70C:

Both alloys are neither enriched nor depleted of metallic Fe in their underlying substrates compared to the bulk composition.

For the low N alloy, both Fe^{2+} and Fe^{3+} are apparently nearer to the metal-film interface, both showing a stronger contribution at 50^{o}.

The high N alloy shows that the Fe^{3+} ion was the majority species in the outer region of the film, i.e., Fe^{3+} is enriched relative to Fe^{2+} at the film-solution interface. The amount of Fe^{3+} in the film of the high N alloy doubles as the temperature is increased from 22 to $70^{o}C$.

3.2.4.7 Ten second passivation at 0mV of 904L alloys in 2M NaCl + 0.1M HCl at 22C:

Both alloys are neither enriched nor depleted of metallic Fe in their underlying substrates compared to the bulk composition. 904LN showed a stronger contribution in the spectra from Fe^{3+} at 50^{o}, i.e., Fe^{3+} is enriched relative to Fe^{2+} at the metal-film interface.

3.2.5 XPS ANALYSIS of N 1s SPECTRA (TABLES 5-18):

3.2.5.1 Ten second passivation at 0mV of AL6X alloys in 2M NaCl + 0.1M HCl at 22C:

From the 50° spectra analysis it is apparent that the underlying substrate of the high N alloy is enriched with nitride; it contains six times more nitride than that of the low N alloy. Since the nitride intensity is more enhanced relative to NH_3 and NH_4^+ in the 50° analysis it is apparently nearer to the metal-film interface than NH_3 or NH_4^+.

The 20° spectra analysis reveals that NH_3 was the majority species for both alloys at this angle which means NH_3 is located primarily at the outer part of the film. NH_4^+ also is located at the outer part of the passive film for both alloys but is observed at a less concentration than that of NH_3. However, the high N alloy has more than three times the amount of NH_4^+ in its film than that of the low N alloy.

3.2.5.2 One hour passivation at 0mV of AL6X alloys in 2M NaCl + 0.1M HCl at 22C:

For both alloys, nitride is evenly distributed throughout their films, although, AL6XN has three times the amount of nitride at 20° or at the outer most part of the film, than does AL6X. Plus, AL6XN has four

times the amount of nitride in the 50° spectra, or inner most part of the film, compared to that of AL6X.

Both alloys show a stronger contribution of the NH_3 species at 20°, suggesting its location at the film-solution interface.

Only the low N alloy showed a strong contribution of NH_4^+. This was revealed in the 20° spectra analysis an implies that this species is at the outer most part of the film.

3.2.5.3 Ten second passivation at 0mV of AL6X alloys in 2M NaCl + 0.1M HCl at 45C:

Both alloys showed a stronger contribution in the spectra from nitride at 50°, i.e., nitride is enriched relative to NH_3 and NH_4^+ at the metal-film interface.

For both alloys NH_3 is the majority species at both angles of take-off, however, it seems to be relatively evenly distributed throughout the films of both alloys according to the spectra.

The 20° spectra analysis shows that NH_4^+ is located at the outermost part of the film for both alloys.

3.2.5.4 One hour passivation at 0mV of AL6X alloys in 2M NaCl + 0.1M HCl at 45C:

The nitride is located at the metal-film interface for both alloys according to the spectra anlysis.

The majority species for both alloys was NH_3 which showed a strong contribution at both take-off angles, but most prevalent in the 20° spectra, indicating its presence to be in the outer part of the films.

NH_4^+ was a very weak contributing species at either angle for either alloy.

3.2.5.5 Ten second passivation at +400mV of AL6X alloys in 0.5M H_2SO_4 at 22C:

The only significant contribution of nitride is observed at 50° of the AL6XN alloy. This implies that the nitride is only located at the innermost part of the film.

NH_3 is present in the films of both alloys at both take-off angles, though the stronger contribution is in the spectra at 20°. This suggests that NH_3 is present throughout the film but at a higher concentration at the outer region of the film.

For each alloy NH_4^+ showed a much stronger contribution in the 20° spectra analysis, hence, its location in the film is apparently nearer to the film-solution interface.

3.2.5.6 Ten second passivation at +400mV of AL6X alloys in 0.5M H_2SO_4 at 70C:

For both alloys, NH_4^+ was the majority species at both 20^o and 50^o angles, however, both alloys showed a stronger contribution in the spectra from NH_4^+ at 20^o, i.e., NH_4^+ is enriched relative to NH_3 and nitride at the film-solution interface. In fact, both alloys have a four-fold increase of NH_4^+ in the outer film region as the temperature increases from 22^o to 70^oC.

Again, NH_3 is distributed throughout the film, but to a greater extent at a higher concentration at the outer part of film.

Nitride makes a small contribution which is observed at 50^o for both alloys; i.e., it is only concentrated at the inner most region of the film.

3.2.5.7 Ten second passivation at 0mV of 904L alloys in in 2M NaCl + 0.1M HCl at 22C:

Nitride is present for both alloys at both angles of take-off, but to a greater extent in the 50^o spectra, indicating its location to be near the metal-film interface.

NH_3 is the majority species for both alloys at both angles relative to nitride and NH_4^+. However, it shows a stronger contribution in the spectra at 20^o.

NH_4^+ is present in a very limited amount for either alloy at either angle.

3.3 COMPARISON OF AL6X/N AND 904L/N IN 2M NaCl+ 0.1M HCl AT 0mV AND 22C:

Comparing atomic percentages of metals from the underlying substrate (50^o spectra) of AL6X/N and 904L/N indicatesd that there is an enrichment of metallic Cr in all the alloys compared to their bulk compositions. However, both 904L and 904LN alloys experience less enrichment compared to their AL6X/N counterparts. The AL6X alloy is 4.3% more enriched with Cr metal in its substrate than the 904L alloy. The AL6XN alloy is 17.1% more enriched than the 904LN alloy.

The 50^o spectral analysis shows there is an enrichment of molybdenum in the underlying substrates of all the alloys compared to their bulk compositions. However, the AL6X alloy has a Mo enrichment that is 51% greater than that of the 904L alloy. AL6XN is also more enriched with metallic Mo than the 904LN alloy, but only by 16.3%.

The underlying substrates of all the alloys have corresponding atomic percentages of Fe which are neither enriched or depleted, but are similar in percentage to their respective bulk compositions.

All the alloys experience a depletion of Ni in their underlying substrate, however, it can be seen that the AL6X/N alloys are more depleted of metallic Ni than the 904L/N alloys compared to their respective bulk compositions. AL6X is more depleted of Ni than 904L by 22.8%, and the AL6XN alloy is more depleted by 26.9% compared to 904LN. When comparing other constituents of the outer region of the films (20^{o} spectra) of AL6X and 904L, it was noticed that 904L contains 1.5 times more $Cr(OH)_3$ than AL6X, but AL6X contains approximately twice as much CrO_3. AL6X also contains 2.75 times more nitride and 2.6 times more NH_3 than 904L. No significant differences were noted in the underlying substrates, i.e., the 50^{o} spectra.

The 20^{o} spectra or outer region of the films of AL6XN and 904LN showed differences in that AL6XN contains 1.75 times more Mo^{6+} and 4.7 times more NH_4^{+}. 904LN contains 1.6 times more CrO_4^{2-}. In their inner region of the films or 50^{o} spectra, it can be seen that AL6XN contains twice the amount of nitride.

3.4 COMPARISON OF AL6X/N IN 2M NaCl + 0.1M HCl AND IN 0.5M H_2SO_4:

3.4.1 AT 22°C:

It can be seen from Tables [20-21] when comparing the atomic percentages from the underlying substrates of the AL6X alloys in the chloride and sulfuric solutions and the AL6XN alloys in those two electrolytes, that they are all similarly enriched by at least 26.3% with metallic Cr compared to the bulk composition. The only major differences of the underlying substrates of the alloys in the different solutions is noted in the amount of Mo in the AL6X alloys and the amount of Ni in the AL6XN alloys. AL6X in the chloride solution has almost 25% more metallic Mo in its substrate, than that in the sulfuric solution. The AL6XN alloy in the chloride solution has 18% less Ni than that in the sulfuric solution.

The important feature in comparing the outer film contents, (20° spectra), of AL6X in the two solutions is that there is twice as much Mo^{4+}, nitride, and H_2O in the outer film region formed in the chloride solution, and there is about twice the amount of $Cr(OH)_3$ and 7.5 times the amount of NH_4^+ in the outer film region formed in sulfuric solution.

The outer regions of the films of AL6XN also

experiences twice the amount of H_2O and 1.4 times the amount of nitride in the chloride solution, and 2.3 times more NH_4^+ in sulfuric solution. The inner film region of AL6XN shows 1.3 times more nitride and three times more H_2O in the chloride solution, and twice the amount of CrO_3 and 3.8 times the amount of NH_4^+ in sulfuric at 22°C.

3.4.2 AT ELEVATED TEMPERATURES OF 45°C in 2M NaCl + 0.1M HCl AND AT 70°C IN 0.5M H_2SO_4:

The important feature to be noticed here, is the difference in amount of NH_4^+ that is generated in the outer region of the films and underlying substrates of the alloys in the different electrolytes. At 70°C, AL6X produces 12.5 times the amount of NH_4^+ in its outer film region in sulfuric solution than in the elevated chloride solution. In the underlying substrate, AL6X develops 15 times the amount of NH_4^+ in sulfuric solution compared to that of the chloride solution.

AL6XN produces 11 times the amount of NH_4^+ in its outer region of film and 10.5 times the amount in its underlying region in the sulfuric solution compared to the chloride solution.

IV. DISCUSSION:

All the alloys examined show similar trends in their metallic atomic percentage contents, regardless of the temperature or electrolyte. All the alloys were enriched with Cr and Mo in their underlying substrate, and all were depleted of Ni in their substrates. None of the alloys showed any significant signs of either depletion or enrichment of their metallic Fe content. The difference in the alloys behavior lies in the extent of their corresponding enrichment or depletion.

It can be seen from Figures 1 and 2 and Tables 2 and 3, that both AL6X and AL6XN are able to reach transpassivity at higher temperatures in the sulfuric solution than in the chloride solution. From Tables [20-21] we can compare the relative amounts of metallic content in the films and substrates of each of the alloys passivated for 10 seconds in the two electrolytes, at the various temperatures.

The atomic percentage concentration of Cr in the substrates of AL6X and AL6XN is 26% in the chloride solution at either room temperature ($22^{o}C$) or the elevated temperature of $45^{o}C$. In the sulfuric solution, the percentage of Cr in the substrates of both alloys is again the same, however, there is a greater enrichment in the sulfuric solution. At $22^{o}C$ and the

elevated temperature of 70°C, the atomic percentage of Cr is 36%.

In the chloride solution at 45°C, there is an enrichment of Cr by 30% in the outer film of both AL6X and AL6XN. At 70°C in the sulfuric solution, the passive film of the high N-alloy is enriched by 18% and the low-N alloy by only 12%.

Ni is similarly depleted in the substrates of both alloys in both solutions at all temperatures by 50%.

The underlying substrates of both AL6X and AL6XN are enriched with Mo by 50% compared to the bulk composition in the chloride solution at each temperature and by 46% in the sulfuric solution at both temperatures. In the chloride solution, the high-N alloy was enriched 10% more with Mo than the low-N alloy at either temperature in their outer films. However, both were 15% more enriched with Mo at 45°C than at room temperature. In the sulfuric solution, the passive films of both alloys were always enriched by 60% compared to the bulk regardless of temperature.

The enrichment of the alloying elements Cr and Mo seems to occur via selective dissolution of Ni during active dissolution. The results here seem to correlate well with Newman's [37] report of elemental Mo inhibiting active dissolution by accumulating on the

active surface, and that of Olefjord and Brox [40] who considered the enrichment of both Mo and Cr on the active surface would reduce the dissolution rate of Cr at the passivation potential. This would allow for the formation of a stable passive film.

Another important observation to be noted is that both AL6X and AL6XN generate much more NH_4^+ in their outer film region in the sulfuric solution than in the chloride solution at both room temperature and at elevated temperatures. At room temperature (22°C), the low-N alloy produces 7.5 times the amount of NH_4^+ in its outer film in sulfuric than it does in the chloride solution. AL6XN generates 2.3 times as much NH_4^+ in the sulfuric solution compared to the chloride solution at 22°C in its outer films.

Also to be noted, is that at room temperature, both alloys have twice the amount of H_2O in their outer films in the chloride solution as they do in the sulfuric.

At the elevated temperature, AL6X in 0.5M H_2SO_4, produces 12.5 times the amount of NH_4^+ in its film and 15 times the amount in its underlying substrate compared to that in the elevated chloride solution. The high-N alloy produces 11 times the amount of NH_4^+ in its outer film and 10.5 times in its substrate in

the sulfuric solution compared to the chloride solution. The increased occurrance of NH_4^+ in the outer films of the alloys in H_2SO_4 solution gives further evidence to Clayton's et. al.[21] theory of the formation of an ammonium sulfate salt layer, which may act as a temporary barrier between the metal and the solution. Of course the formation of NH_4^+ would also tend to lower the local surface solution acidity as noted previously [10,19 and 21].

The passive films formed on 904L/N at 0mV for 10 seconds in 2M NaCl + 0.1M HCl were studied to compare the results to those of the AL6X/N alloys to evaluate the behavior of N with varying atomic percentages of Mo.

From the passive films formed on the alloys, it can be seen that there is an enrichment of the alloying elements Cr and Mo in the outer films of all the alloys. All are similarly enriched with metallic Mo, but the AL6X/N alloys have a greater enrichment of Cr compared to the 904L/N alloys. AL6X is approximately 10% more enriched and AL6XN is about 15% more enriched compared to their 904L counterparts.

All alloys were similarly depleted of Ni in their films by 22%. However, the AL6X/N alloys were also Fe-depleted. AL6X by 6% and AL6XN by 14.4%.

When looking at the underlying substrates of each of the four alloys, it is observed that all the alloys experience an enrichment of both Cr and Mo, however, the AL6X/N alloys are again, more enriched with both alloying elements.

All alloys are also depleted of Ni in their underlying substrates, however AL6X/N alloys are both approximately 25% more depleted than that of the 904L/N alloys.

None of the alloys show depletion or enrichment of their Fe content.

Therefore, it seems that a 2% increase in the Mo content of an alloy with the same amount of N, increases the selective dissolution of Ni and provides for a greater enrichment of Mo and Cr, and Cr is a very important element in the forming of a strong barrier layer in the passive film. Also to be noted, is that an alloy with the same amount of N as another but a higher Mo content has a greater concentration of nitride, NH_3 and NH_4^+ in its outer film. It seems as though the enhanced enrichment provides a stronger barrier layer which decreases the dissolution rate of the alloy and allows for the formation of a more complete passive film.

V. CONCLUSIONS:

1. Increasing the N content of both the AL6X and the 904L alloys from 0.04 to 0.20 wt% improves the pitting resistance and the passivation characteristics of each in 2M NaCl + 0.1M HCl and 0.5M H_2SO_4 solutions at both room and and elevated temperatures. However, the N seems to be more effective in the sulfuric solution.

2. The AL6X alloys with their 1.8 wt% greater Mo content, showed a much greater effect of pitting resistance and improved passivation characteristics compared to the 904L alloys. This suggests a strong Mo-N synergistic effect.

3. XPS analysis shows a greater surface enrichment of metallic Cr and Mo and a greater surface depletion of Ni in the films of the AL6X/N alloys. This seems to occur via selective active dissolution of Ni and the impedence of passive dissolution by metallic Mo allowing a strong Cr barrier layer to form.

4. In sulfuric solution, the increase of NH^4 formation appears to be the result of the formation of an ammonium sulfate salt layer which acts as a barrier layer.

5. Further XPS analysis of the alloys after polarizing at their critical current densities may give some indication to the mechanism(s) at work, for the most noticeable difference between the alloys is seen in this anodic region. Unfortunately, instrument failure has prevented any investigation of this type as of yet.

VI. FUTURE WORK:

Unfortunately, due to instrument failure, a more thorough investigation could not be conducted. XPS analysis of the alloys at their passivation potential, the region of the anodic nose on the polarization curves, needs to be examined . For here, the critical current density varied significantly between alloys, solutions and solution temperatures. Further work with the 904L alloys has to be carried out in order to compare the results with the higher Mo alloys, AL6X. It would be interesting to see if 904L, which has the same N content as AL6X, would produce as much NH^4 in sulfuric solution as AL6X even though its Mo content is less. Within these investigations, a mechanism for the apparent synergistic effect may be resolved.

REFERENCES

[1] B. Gunia and G.R. Woodrow, J. Mater., 5, 413, 1970.

[2] L.A. Norstrom, Metal Sci., 11, 208, 1977.

[3] J.K. Solberg, Mat. Sci. and Eng., 55, 39, 1982.

[4] T. Ogawa, K. Suzuki and T. Zaien, Weld. J., 63, 213-s, 1984.

[5] W.T. Delong, Weld. J., 53 (7), 273-s, 1974.

[6] J.R. Kearns, "The Effect of Nitrogen on the Corrosion Resistance of Austenitic Stainless Alloys Containing Molybdenum.", Michigan, Sept., 1984.

[7] J.R. Kearns and H.E. Deverell, "The Use of Nitrogen to Improve Fe-Cr-Ni-Mo Alloys for the Chemical Process Industries," CORROSION/86, Paper No.188, NACE, Houston, TX, 1984.

[8] A.J. Sedriks, Corr., 42 (7), 376, 1986.

[9] U. Kamachi Mudali, R.K. Dayal, T.P.S. Gill and J.B. Gnanamoorthy, Werk. Korr., 37, 637, 1986.

[10] K. Osozawa and N. Okato, Passivity and Its Breakdown on Iron and Iron Base Alloys, R.W. Staehle and H. Okada (eds.), NACE, Houston, TX, 135, 1976.

[11] R. Bandy and D. Van Rooyen, Corr., 39 (6), 227, 1983.

[12] R. Bandy and D. Van Rooyen, Corr., 41 (4), 228, 1985.

[13] J.J.Eckenrod and C.W. Kovach, ASTM STP., 679, 17,1977.

[14] M.A. Streicher, J. Electrochem. Soc., 103 (7), 375, 1956.

[15] J.E. Truman, M.J. Coleman and K.T. Pirt, Br. Corrs. J., 12 (4), 236, 1977.

[16] A.G. Hartline III, Metall. Trans., 5, 2271, 1974.

[17] M. Janik-Czachor, E. Lunarska and Z. Szklarska-Smialowska, Corr., 31 (11), 394, 1975.

[18] Y.A. Kolotyrkin, in Internaional Congress on Metallic Corrosion, June 1984, Proceedings, Vol.I, Toronto, Canada, 1984.

[19] V. Chigal, V.M. Knyazheva, Ya. Pitter, S.G. Babich and S.D. Bogolyuloskii, Prot. of Met., 22 (2), 164, 1986.

[20] R.C. Newman and M.A.A. Ajjawi, Corr. Sci., 26 (12), 1057,1986.

[21] C.R. Clayton, L. Rosenzweig, M. Oversluizen and Y.C. Lu, in "Surfaces, Inhibition and Passivation," eds. E. McCafferty and T. Brodd, The Electrochemical Society, Pennington, NJ, 1986, 323.

[22] R.C. Newman, Y.C. Lu, R. Bandy and C.R. Clayton, Proc. Ninth Inter. Cong. Metallic Corrosion, Vol.3, Toronto, 394, 1983.

[23] R. Bandy, Y.C. Lu, R.C. Newman and C.R. Clayton, Proc. Equilibrium Diagrams and Localized Corrosion Symp., R. Frankenthal and J. Kruger (eds.), The Electrochemical Society, Pennington, NJ, 1984, 471.

[24] R.F.A. Jargelius, "The Influence of Nitrogen Alloying on the Corrosion Resistance of 20Cr25Ni and 20Cr25Ni4.5Mo Stainless Steels," Swedish Institute for Metals, Research Report IM-2179, 1986.

[25] Y.C. Lu, C.R. Clayton, R. Bandy and R.C. Newman, J. Electrochem. Soc., 1774, 1983.

[26] J. Kolts, J.B.C. Wu and A.I. Asphahani, Metal Prog., 124, 25, 1983.

[27] R.C. Newman and T. Shahriba, Corr. Sci., 27 (8), 827, 1987.

[28] T. Ogawa, S. Aoki, T. Sakamoto and T. Zaizen, Welding J., 61, 139s, 1982.

[29] C.R. Clayton and K.G. Martin, Proc. Int. Conf. on High Nitrogen Steel, Lille, France, 1988. Inst. of Metals, London U.K., To be published.

[30] T. Fukuzuka, "Corrosion Resistance to Sea Water of High Molybdenum Austenitic Stainless Steel (20Cr22Ni5Mo0.2N)," Kobe Steel Interim Report, Oct., 1979.

[31] R.J. Brigham, Corr., 30 (11), 396, 1974.

[32] R.J. Brigham and E.W. Tozer, Corr., 29 (1), 33, 1973.

[33] Z. Szklarska-Smialowska and Mankowski, Corr. Sci., 12, 925, 1972.

[34] K. Sugimoto and Y. Sawada, Corr., 32 (9), 347, 1976.

[35] K. Hashimoto and K. Asami, Corr. Sci., 19, 251, 1979.

[36] R.C. Newman, Corr. Sci., 25 (5), 331, 1985.

[37] R.C. Newman, Corr. Sci., 25 (5), 341, 1985.

[38] Y.C. Lu and C.R. Clayton, J. Electrochem. Soc., 132 (10), 2517, 1985.

[39] C.R. Clayton and Y.C. Lu, J. Electrochem. Soc., 133 (12), 2465, 1986.

[40] I. Olefjord and B. Brox, Proceedings of fifth International Symposium on Passivity, Bombannes, France, 1983.

[41] I. Olefjord and B.O. Elfstrom, Corr., 38 (1), Jan. 1982.

[42] H. Ogawa, H. Omata, I. Itoh, H. Okada, Corr., 34 (2), 52, 1978.

[43] K. Hashimoto, K. Asami and K. Teramoto, Corr. Sci., 19, 3, 1979.

[44] F.A. Lizlovs and A.P. Bond, J. Electrochem. Soc., 116, 574, 1969.

[45] J.E. Castel and C.R. Clayton, Corr. Sci, 17, 7, 1977.

[46] A. Savitsky and M.J.E. Golay, Anal. Chem., 36, 1627, 1964.

[47] P. Sherwood, in "Practical Surface Analysis," eds. D. Briggs and M.P. Seah, John Wiley & Sons, Inc., New York, 1983, p.445.

TABLE 1 Chemical Compositions of AL6X and 904L Stainless Steels

	AL6X	AL6XN	904L	904LN
C	0.020	0.020	0.019	0.024
Mn	1.47	1.63	1.50	1.50
P	0.030	0.021	0.023	0.024
S	0.002	0.002	0.002	0.002
Si	0.50	0.43	0.44	0.52
Cr	20.45	20.68	20.46	20.33
Ni	24.65	24.78	24.40	24.58
Mo	6.30	6.30	4.51	4.50
Cu	0.19	0.18	1.48	1.50
N	0.042	0.190	0.053	0.200

Compositions in weight percent

TABLE 2: Electrochemical Characteristics of AL6X Stainless Steels

2M NaCl + 0.1M HCl pH 0.7

		AL6X	AL6XN
22°C	Ecorr(mV)	-306	-306
	Epp(mV)	-248	-250
	Icrit(uA/cm^2)	26.36	20.18
	Ipass(uA/cm^2)	3.88	3.79
	Epit(mV)	-	-
	Etrans(mV)	860	860
37°C	Ecorr(mV)	-327	-328
	Epp(mV)	-287	-247
	Icrit(uA/cm^2)	39.66	22.90
	Ipass(uA/cm^2)	6.06	4.14
	Epit(mV)	-	-
	Etrans(mV)	840	850
40°C	Ecorr(mV)	-312	-310
	Epp(mV)	-268	-269
	Icrit(uA/cm^2)	56.40	36.50
	Ipass(uA/cm^2)	5.15	4.95
	Epit(mV)	291	-
	Etrans(mV)	-	840
42°C	Ecorr(mV)	-306	-358
	Epp(mV)	-265	-306
	Icrit(uA/cm^2)	39.90	75.95
	Ipass(uA/cm^2)	5.47	3.67
	Epit(mV)	271	-
	Etrans(mV)	-	796
45°C	Ecorr(mV)	-330	-306
	Epp(mV)	-281	-237
	Icrit(uA/cm^2)	68.90	91.10
	Ipass(uA/cm^2)	5.44	4.92
	Epit(mV)	123	265
	Etrans(mV)	-	-

TABLE 3: Electrochemical Characteristics of AL6X Stainless Steels

0.5M H_2SO_4 pH 0.4

		AL6X	AL6XN
22°C	Ecorr(mV)	-283	-350
	Epp(mV)	-131	-185
	Icrit(uA/cm^2)	34.85	15.04
	Ipass(uA/cm^2)	5.08	4.34
	Etrans	837	852
50°C	Ecorr(mV)	-297	-306
	Epp(mV)	-201	-201
	Icrit(uA/cm^2)	70.30	63.20
	Ipass(uA/cm^2)	8.87	8.38
	Etrans(mV)	820	848
70°C	Ecorr(mV)	-297	-322
	Epp(mV)	-245	-249
	Icrit(uA/cm^2)	178.80	77.20
	Ipass(uA/cm^2)	8.72	8.02
	Etrans(mV)	812	832
75°C	Ecorr(mV)	-306	-274
	Epp(mV)	-237	-219
	Icrit(uA/cm^2)	252.00	56.67
	Ipass(uA/cm^2)	9.00	8.25
	Etrans(mV)	800	828
85°C	Ecorr(mV)	-297	-291
	Epp(mV)	-249	-185
	Icrit(uA/cm^2)	448.00	83.10
	Ipass(uA/cm^2)	11.97	9.19
	Etrans(mV)	812	824

TABLE 4: Electrochemical Characteristics of 904L Stainless Steels

2M NaCl + 0.1M HCl pH 0.7

		904L	904LN
22°C	Ecorr(mV)	-314	-340
	Epp(mV)	-201	-228
	Icrit(uA/cm^2)	118.0	103.0
	Ipass(uA/cm^2)	4.07	3.62
	Epit(mV)	-	-
	Etrans(mV)	830	848
37°C	Ecorr(mV)	-318	-304
	Epp(mV)	-169	-231
	Icrit(uA/cm^2)	306.0	204.6
	Ipass(uA/cm^2)	10.11	4.64
	Epit(mV)	335	-
	Etrans(mV)	-	870
40°C	Ecorr(mV)	-328	-318
	Epp(mV)	-223	-200
	Icrit(uA/cm^2)	153.7	136.2
	Ipass(uA/cm^2)	4.81	4.16
	Epit(mV)	157	191
	Etrans(mV)	-	-
45°C	Ecorr(mV)	-306	-326
	Epp(mV)	-237	-269
	Icrit(uA/cm^2)	407.0	228.0
	Ipass(uA/cm^2)	9.41	5.73
	Epit(mV)	143	147
	Etrans	-	-

TABLE 5: Normalised Integrated Peak Areas for the main spectra obtained from the passive films formed on AL6X/N in 2M NaCl + 0.1M HCl at 0mV (SCE) for 10 seconds at 22C.

		AL6X		AL6XN	
		20°	50°	20°	50°
Cr 2p	Cr(metal)	3.8	11.8	6.0	21.5
	Cr_2O_3	19.6	18.9	22.0	23.7
	$Cr(OH)_3$	24.1	24.2	35.6	27.8
	CrO_3	8.3	4.8	6.0	3.5
	CrO_4^{2-}	5.0	3.6	2.7	3.8
Mo 3d	Mo(metal)	1.1	5.2	1.9	6.7
	Mo^{4+}	2.0	2.1	2.8	2.4
	Mo^{6+}	7.8	7.0	10.5	7.6
N 1s	Nitride	1.1	0.4	1.3	2.4
	NH_3	3.7	1.9	4.2	2.8
	NH_4^+	0.4	0.6	1.4	0.5
Fe 2p	Fe(metal)	7.1	20.5	9.0	33.9
	Fe^{3+}	14.7	17.3	10.2	14.0
	Fe^{2+}	18.4	22.0	10.3	17.3
Ni 2p	Ni(metal)	6.8	14.0	9.2	17.9
O 1s	O^{2-}	15.4	40.6	31.9	45.6
	OH^-	105.3	84.1	104.6	74.6
	H_2O	59.2	19.7	66.3	30.3

TABLE 6: Normalized Integrated Peak Areas for the main spectra obtained from the passive films formed on AL6X/N in 2M NaCl + 0.1M HCl at 0mV (SCE) for 1 hour at 22C.

		AL6X		AL6XN	
		20°		50°	
Cr 2p	Cr(metal)	9.5	22.2	8.4	23.3
	Cr_2O_3	18.7	16.1	23.8	25.8
	$Cr(OH)_3$	41.6	32.8	36.9	27.0
	CrO_3	9.1	2.3	6.9	6.0
	CrO_4^{2-}	4.3	2.3	3.9	3.6
Mo 3d	Mo(metal)	3.6	7.0	3.2	7.1
	Mo^{4+}	3.1	2.6	1.3	1.2
	Mo^{6+}	8.1	6.2	5.9	4.9
N 1s	Nitride	0.4	0.5	1.2	1.9
	NH_3	2.6	1.6	3.9	3.1
	NH_4^+	1.1	0.8	0.4	0.4
Fe 2p	Fe(metal)	16.2	47.9	11.7	31.1
	Fe^{2+}	7.0	15.0	10.0	15.4
	Fe^{3+}	8.1	19.7	11.3	16.1
Ni 2p	Ni(metal)	19.1	43.7	6.7	17.1
O 1s	O^{2-}	35.2	36.9	43.8	54.4
	OH^-	108.6	82.7	119.7	86.1
	H_2O	35.9	25.9	76.7	41.1

TABLE 7: Normalized Integrated Peak Areas for the main spectra obtianed from the passive films formed on AL6X/N in 2M NaCl + 0.1M HCl at 0mV (SCE) for 10 seconds at 45C.

		AL6X		AL6XN	
		20°	50°	20°	50°
Cr 2p	Cr(metal)	9.5	18.7	13.2	24.9
	Cr_2O_3	19.5	22.2	16.8	20.7
	$Cr(OH)_3$	28.5	25.0	32.3	24.0
	CrO_3	7.4	3.4	5.5	5.7
	CrO_3	2.1	2.3	4.2	2.9
Mo 3d	Mo(metal)	4.0	6.7	4.6	9.3
	Mo^{4+}	1.9	2.3	7.6	2.3
	Mo^{6+}	10.5	8.1	10.2	8.0
N 1s	Nitride	0.6	1.1	1.7	2.8
	NH_3	2.5	2.0	8.7	5.6
	NH_4^+	1.0	0.4	1.2	0.6
Fe 2p	Fe(metal)	15.7	34.0	21.0	47.3
	Fe^{2+}	15.2	18.2	13.0	16.5
	Fe^{3+}	14.9	18.5	10.4	16.6
Ni 2p	Ni(metal)	9.9	20.5	14.7	31.8
O 1s	O^{2-}	36.6	41.0	44.5	48.4
	OH^-	93.8	80.3	90.1	88.3
	H_2O	35.1	19.5	48.3	30.8

TABLE 8: Normalised Integrated Peak Areas for the main spectra obtianed from the passive films formed on AL6X/N in 2M NaCl + 0.1M HCl at 0mV for 1 hour at 45C.

		AL6X		AL6XN	
		20°	50°	20°	50°
Cr 2p	Cr(metal)	9.1	22.7	10.0	19.6
	Cr_2O_3	22.7	23.9	28.7	25.6
	$Cr(OH)_3$	35.0	27.4	31.2	29.1
	CrO_3	6.9	5.3	7.2	5.4
	CrO_4^{2-}	4.5	2.4	4.0	2.2
Mo 3d	Mo(metal)	3.7	6.8	3.5	6.5
	Mo^{4+}	1.9	1.6	2.3	2.2
	Mo^{6+}	7.5	5.9	6.5	5.8
N 1s	Nitride	0.4	1.3	1.4	2.5
	NH_3	4.1	2.3	5.5	2.5
	NH_4^+	0.4	0.3	0.5	0.2
Fe 2p	Fe(metal)	17.8	43.8	18.4	41.1
	Fe^{2+}	10.8	18.0	9.9	14.9
	Fe^{3+}	10.7	15.7	10.2	14.7
Ni 2p	Ni(metal)	14.6	34.0	18.5	28.8
O 1s	O^{2-}	47.2	54.1	47.7	55.4
	OH^-	102.9	73.0	93.6	82.7
	H_2O	34.1	23.2	31.2	24.6

TABLE 9: Normalised Integrated Peak Areas for the main spectra obtained from the passive films formed on AL6X/N in 0.5M H_2SO_4 at +400mV (SCE) for 10 seconds at 22C.

		AL6X		AL6X	
		20°	50°	20°	50°
Cr 2p	Cr(metal)	8.0	19.8	7.0	21.7
	Cr_2O_3	17.1	20.5	14.3	18.4
	$Cr(OH)_3$	40.9	28.2	38.1	27.5
	CrO_3	7.6	6.6	9.7	7.3
	CrO_4^{2-}	4.7	2.5	4.5	3.3
Mo 3d	Mo(metal)	3.5	6.6	2.8	6.3
	Mo^{4+}	1.0	2.5	2.3	2.7
	Mo^{6+}	5.1	6.3	7.5	5.4
N 1s	Nitride	0.6	0.7	0.9	1.8
	NH_3	2.0	1.4	4.6	2.3
	NH_4^+	3.0	0.9	3.2	1.9
Fe 2p	Fe(metal)	12.4	36.4	13.4	35.3
	Fe^{2+}	13.1	14.1	11.2	16.7
	Fe^{3+}	10.5	19.3	12.4	18.7
Ni 2p	Ni(metal)	8.9	23.2	10.5	23.0
O 1s	O^{2-}	42.2	47.9	35.4	40.6
	OH^-	92.2	63.1	77.0	67.1
	SO_4^{2-}	69.7	40.7	66.4	39.1
	H_2O	29.2	10.8	23.4	10.7

TABLE 10: Normalized Integrated Peak Areas for the main spectra obtained from the passive films formed on AL6X/N in 0.5M H_2SO_4 at +400mV (SCE) for 10 seconds at 70C.

		AL6X		AL6XN	
		20°	50°	20°	50°
Cr 2p	Cr(metal)	5.6	20.0	13.5	18.0
	Cr_2O_3	12.4	6.8	10.6	23.2
	$Cr(OH)_3$	44.7	21.4	38.8	2[illegible].1
	CrO_3	7.9	6.3	8.4	[illegible].8
	CrO_4^{2-}	5.4	4.3	7.6	3.0
Mo 3d	Mo(metal)	3.4	6.3	6.8	7.1
	Mo^{4+}	1.8	1.7	3.2	3.1
	Mo^{6+}	6.5	4.1	4.7	5.2
N 1s	Nitride	0.9	1.6	1.4	1.8
	NH_3	3.4	1.3	6.3	3.8
	NH_4^+	12.5	6.0	13.2	6.3
Fe 2p	Fe(metal)	9.1	32.8	27.4	35.3
	Fe^{2+}	11.7	24.7	9.0	15.5
	Fe^{3+}	9.5	30.7	17.7	16.1
Ni 2p	Ni(metal)	15.0	23.2	19.0	23.8
O 1s	O^{2-}	19.7	10.8	14.6	36.0
	OH^-	89.8	49.5	60.5	72.5
	SO_4^{2-}	91.9	91.6	215.7	45.7
	H_2O	54.8	21.9	53.3	19.6

TABLE 11: Normalized Integrated Peak Areas for the main spectra obtained from the passive films formed on 904L/N in 2M NaCl + 0.1M HCl at 0mV (SCE) for 10 seconds at 22C.

		AL6X		AL6XN	
		20°	50°	20°	50°
Cr 2p	Cr(metal)	7.4	21.0	6.3	17.3
	Cr_2O_3	12.5	16.7	18.2	20.3
	$Cr(OH)_3$	38.5	28.6	31.6	21.2
	CrO_3	4.4	3.6	6.5	4.8
	CrO_4^{2-}	4.2	1.5	2.0	2.0
Mo 3d	Mo(metal)	2.1	4.7	2.0	5.5
	Mo^{4+}	1.8	1.4	1.8	2.9
	Mo^{6+}	6.5	0.4	6.0	7.0
N 1s	Nitride	0.4	0.8	1.0	1.2
	NH_3	1.4	1.5	3.5	2.4
	NH_4^+	0.5	0.4	0.3	0.8
Fe 2p	Fe(metal)	17.3	39.9	13.0	35.0
	Fe^{2+}	12.3	18.0	18.5	19.9
	Fe^{3+}	17.5	20.5	15.5	22.0
Ni 2p	Ni(metal)	13.6	34.1	10.7	23.7
O 1s	O^{2-}	28.1	41.1	43.9	40.7
	OH^-	104.0	71.2	107.8	72.9
	H_2O	48.2	25.0	29.0	20.9

TABLE 12: Normalized Integrated Peak Area Ratios obtained from the passive films formed on AL6X/N in 2M NaCl + 0.1M HCl at 0mV for 10s and 1 hr at 22C.

10s	AL6X		AL6XN	
	20°	50°	20°	50°
$>Cr^{n+}/>Fe^{n+}$	1.7	1.3	3.2	1.9
$>Mo^{n+}/>Fe^{n+}$	0.3	0.2	0.6	0.3
$Cr_2O_3/Cr(OH)_3$	0.8	0.8	0.6	0.9
Fe^{3+}/Fe^{2+}	1.3	1.3	1.0	1.2
O^{2-}/OH^-	0.1	0.5	0.3	0.6
1 hour				
$>Cr^{n+}/>Fe^{n+}$	4.9	1.6	3.4	2.0
$>Mo^{n+}/>Fe^{n+}$	0.7	0.3	0.3	0.2
$Cr_2O_3/Cr(OH)_3$	0.4	0.5	0.6	0.1
Fe^{3+}/Fe^{2+}	1.3	1.3	1.0	1.0
O^{2-}/OH^-	0.4	0.4	0.6	0.6

TABLE 13: Normalized Integrated Peak Area Ratios obtained from the passive films formed on Al6X/N in 2M NaCl + 0.1M HCl at 0mV for 10s and 1 hr at 45C.

10 sec.	AL6X		AL6XN	
	20^{o}	50^{o}	20^{o}	50^{o}
$>Cr^{n+}/>Fe^{n+}$	1.9	1.4	2.5	1.6
$>Mo^{n+}/>Fe^{n+}$	0.4	0.3	0.8	0.4
$Cr_2O_3/Cr(OH)_3$	0.7	0.9	0.5	0.9
Fe^{3+}/Fe^{2+}	0.9	1.0	0.8	1.0
O^{2-}/OH^{-}	0.4	0.5	0.5	0.5
1 hour				
$>Cr^{n+}/>Fe^{n+}$	3.2	1.8	3.5	2.1
$>Mo^{n+}/>Fe^{n+}$	0.4	0.9	0.4	0.3
$Cr_2O_3/Cr(OH)_3$	0.6	0.9	0.9	0.9
Fe^{3+}/Fe^{2+}	0.9	0.8	1.0	0.9
O^{2-}/OH^{-}	0.5	0.7	0.5	0.7

TABLE 14: Normalized Integrated Peak Area Ratios obtained from the passive films formed on AL6X/N in 0.5M H_2SO_4 at +400mV for 10s at 22C and 70C.

22°C	AL6X		AL6XN	
	20°	50°	20°	50°
$>Cr^{n+}/>Fe^{n+}$	3.0	1.7	2.8	1.6
$>Mo^{n+}/>Fe^{n+}$	0.3	0.3	0.4	0.2
Cr_2O_3	0.4	0.7	0.4	0.7
Fe^{3+}/Fe^{2+}	0.8	1.4	1.1	1.1
O^{2-}/OH^-	0.5	0.8	0.5	0.6
70°C				
$>Cr^{n+}/>Fe^{n+}$	3.3	0.7	2.4	1.9
$>Mo^{n+}/>Fe^{n+}$	0.4	0.2	0.3	0.3
$Cr_2O_3/Cr(OH)$	0.3	0.3	0.3	0.8
Fe^{3+}/Fe^{2+}	0.8	1.2	2.0	1.0
O^{2-}/OH^-	0.2	0.2	0.2	0.2

TABLE 15: Normalized Integrated Peak Area Ratios obtained from the passive films formed on 904L/N in 2M NaCl + 0.1M HCl at 0mV for 10s at 22C.

	904		904L	
	20°	50°	20°	50°
$>Cr^{n+}/>Fe^{n+}$	2.0	1.3	1.7	1.2
$>Mo^{n+}/>Fe^{n+}$	0.3	0.2	0.2	0.2
$Cr_2O_3/Cr(OH)_3$	0.3	0.6	0.6	0.9
Fe^{3+}/Fe^{2+}	1.4	1.1	0.8	1.1
O^{2-}/OH^-	0.3	0.6	0.4	0.6

TABLE 16: Atomic percentages of metals from underlying substrate obtained from the passive films formed on AL6X and AL6XN in 2M NaCl + 0.1M HCl at 0mV (SCE) for 10s and 1hr at 22 and 45 degrees Celsius.

		AL6X	AL6XN
(22°)	10s:	Cr= 30.0%	33.9%
		Mo= 9.8%	8.0%
		Fe= 45.3%	46.4%
		Ni= 14.9%	11.7%
	1 hr:	Cr= 25.5%	37.0%
		Mo= 5.9%	8.6%
		Fe= 47.8%	43.0%
		Ni= 20.8%	11.3%
(45°C)	10s:	Cr= 30.2%	28.9%
		Mo= 8.2%	8.1%
		Fe= 47.8%	47.7%
		Ni= 13.8%	15.3%
	1 hr:	Cr= 28.5%	27.1%
		Mo= 6.4%	6.7%
		Fe= 47.5%	49.4%
		Ni= 17.5%	16.7%

Bulk atomic % of alloys: Cr= 22.1%
Mo= 4.0%
Fe= 47.8%
Ni= 25.9%

TABLE 17: Atomic percentages of metals from underlying substrate obtained from the passive films formed on AL6X and AL6XN in 0.5M H_2SO_4 at 400mV (SCE) for 10 secs at 22C and 70C.

		AL6X	AL6XN
(22°C)	10s:	Cr= 29.9%	32.6%
		Mo= 7.5%	7.0%
		Fe= 48.0%	46.1%
		Ni= 14.6%	14.3%
(70°C)	10s:	Cr= 28.2%	31.8%
		Mo= 8.4%	7.5%
		Fe= 48.0%	45.3%
		Ni= 15.5%	15.3%

Bulk atomic % of alloys: Cr= 22.1%
Mo= 4.0%
Fe= 47.8%
Ni= 25.9%

TABLE 18: Atomic percentages of metals from underlying substrate obtained from the passive films formed on 904L and 904LN in 2M NaCl + 0.1M HCl at 0mV (SCE) for 10 seconds at 22C.

		904L	904LN
(22°C)	10s:	Cr= 28.7%	28.1%
		Mo= 4.8%	6.7%
		Fe= 47.2%	49.3%
		Ni= 19.3%	16.0%

Bulk atomic % of alloys: Cr= 23.3%
Mo= 2.7%
Fe= 49.5%
Ni= 24.3%

TABLE 19

Peak Synthesis Parameters for N 1s and Mo 3p 3/2

Chemical Species	B.E.	FWHM	G/L	T.H.	T.S.	T.M.
Nitride	397.2	1.8	50	5	.1	5
NH_3	399.8	1.7	50	5	.1	5
NH_4^+	401.7	1.7	50	5	.1	5
Mo metal	393.6	2.5	80	70	.05	5
Mo^{4+}	395.1	2.9	50	5	.1	5
Mo^{6+}	397.6	2.9	50	5	.1	5

Peak Synthesis Parameters for Fe 2p 3/2

Fe metal	706.8	1.8	50	70	.08	5
Fe^{2+}	709.0	2.2	50	70	.1	5
Fe^{3+}	710.9	2.4	50	70	.05	5

All Binding Energies are + 0.1 eV

B.E. = Binding Energy (eV)
FWHM = Full Width Half Maximum
G/L = Gaussian/Lorentzian Mixing Ratio (% Lorentzian)
T.H. = Tail Height %
T.S. = Slope Exponential Tail
T.M. = Tail Mixing Ratio (% Linear)

TABLE 20

Peak Synthesis Parameters for Cr 2p 3/2

Chemical Species	B.E.	FWHM	G/L	T.H.	T.S.	T.M.
Metal 2p 3/2	574.1	1.7	65	15	.05	5
Metal 2p 1/2	583.3	2.1	80	50	.05	5
Cr_2O_3	576.3	2.2	50	10	.1	5
$Cr(OH)_3$	577.0	2.2	50	10	.1	5
CrO_3	578.1	1.3	50	10	.1	5
CrO_4^{2-}	579.3	1.2	50	10	.1	5

Metal 2p 3/2 : 2p 1/2 peak area ratio = 2:1

Peak Synthesis Parameters for Mo 3d

Metal 3d 5/2	227.7	1.1	80	25	.05-.1	5
Metal 3d 3/2	230.9	1.4	90	70	.1	5
Mo^{4+}3d 5/2	230.2	1.9	50	10	.1	5
Mo^{4+}3d 3/2	233.4	2.1	50	10	.1	5
Mo^{6+}3d 5/2	231.9	2.0	50	10	.1	5
Mo^{6+}3d 3/2	235.1	2.1	50	10	.1	5
SO_4^{2-}	232.5	2.5	20	10	.05	5

All Binding Energies are + 0.1 eV

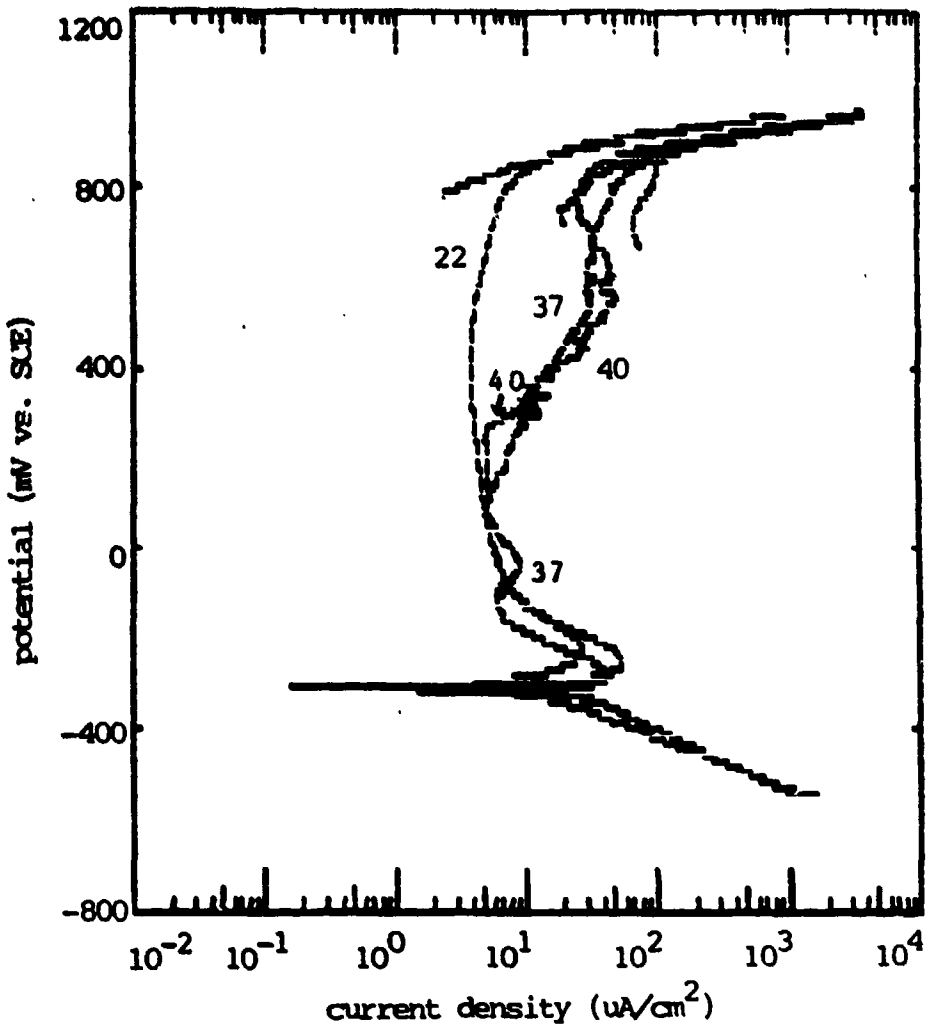

Figure 1: Comparison of the polarization curves of AL6X ss containing 0.04 wt% N in 2M NaCl+ 0.1M HCl at 22, 37 and 40 degrees Celsius.

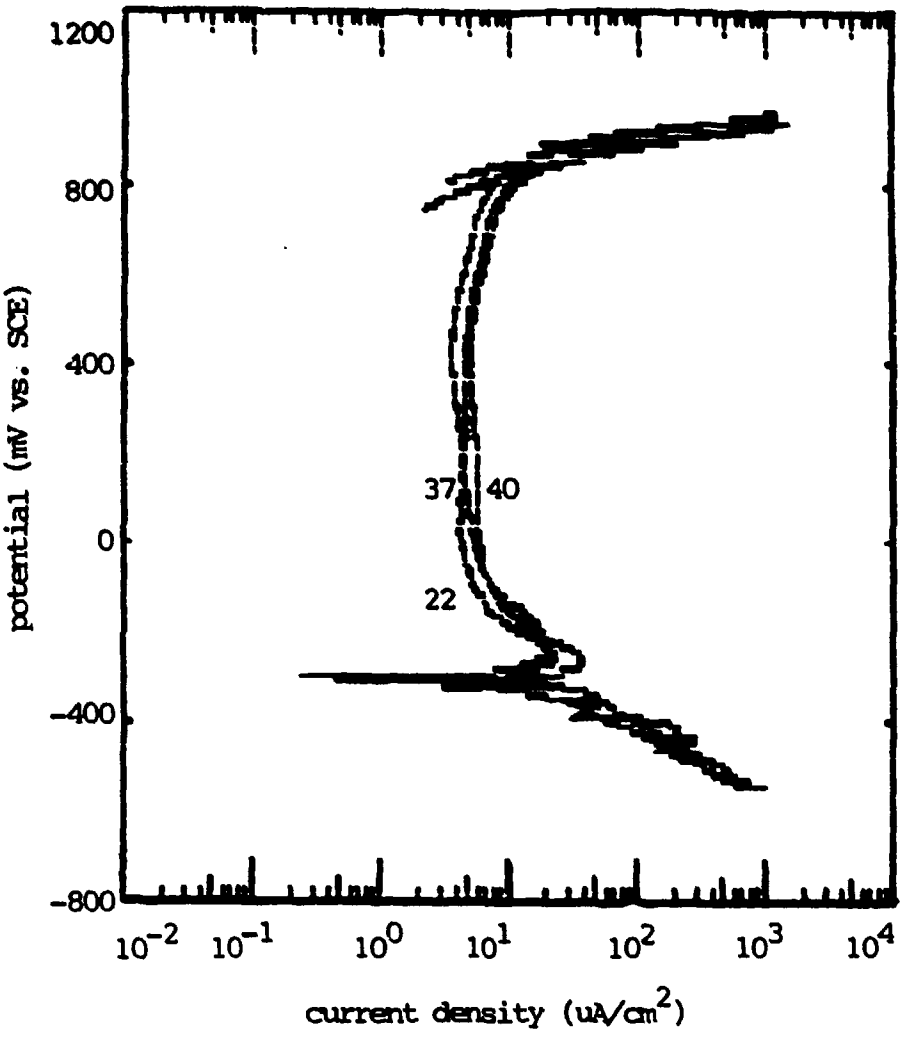

Figure 2: Comparison of the polarization curves of AL6XN ss containing 0.19 wt% N in 2M NaCl + 0.1M HCl at 22, 37 and 40 degrees Celsius.

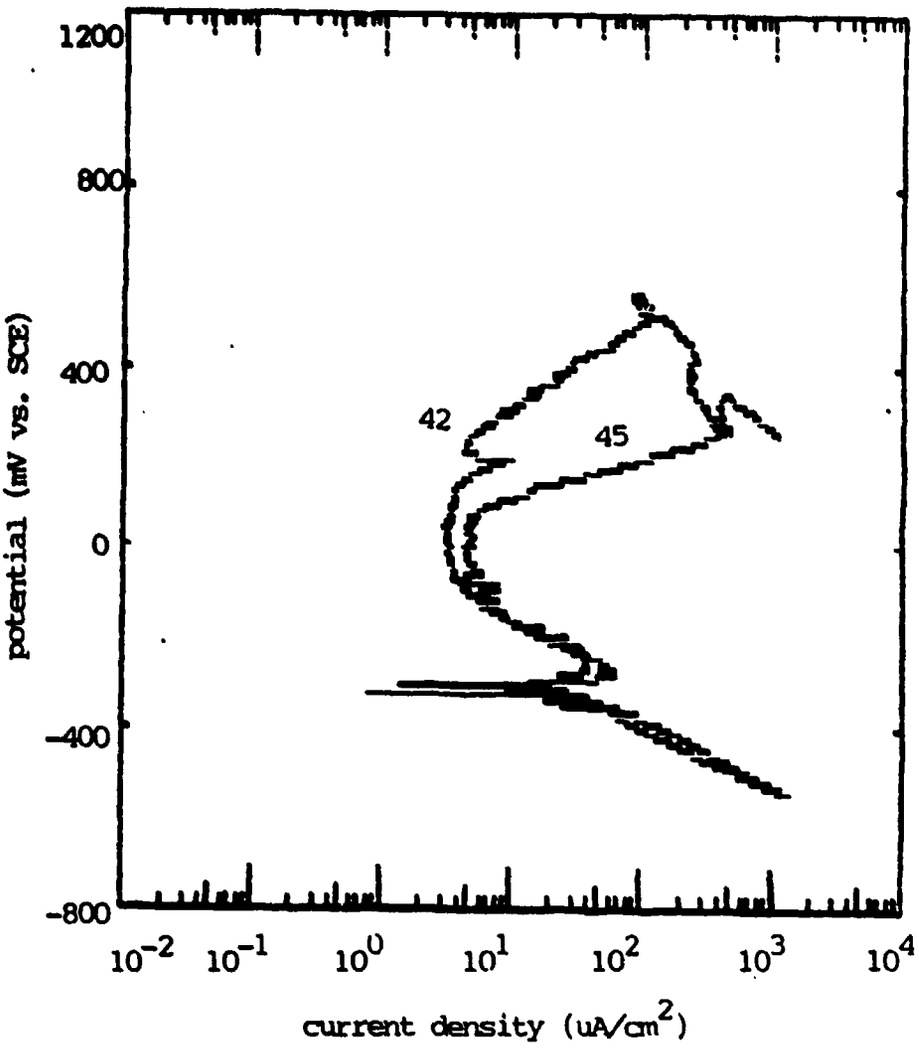

Figure 3: Comparison of the polarization curves of AL6X ss containing 0.04 wt% N in 2M NaCl + 0.1M HCl at 42 and 45 degrees Celsius.

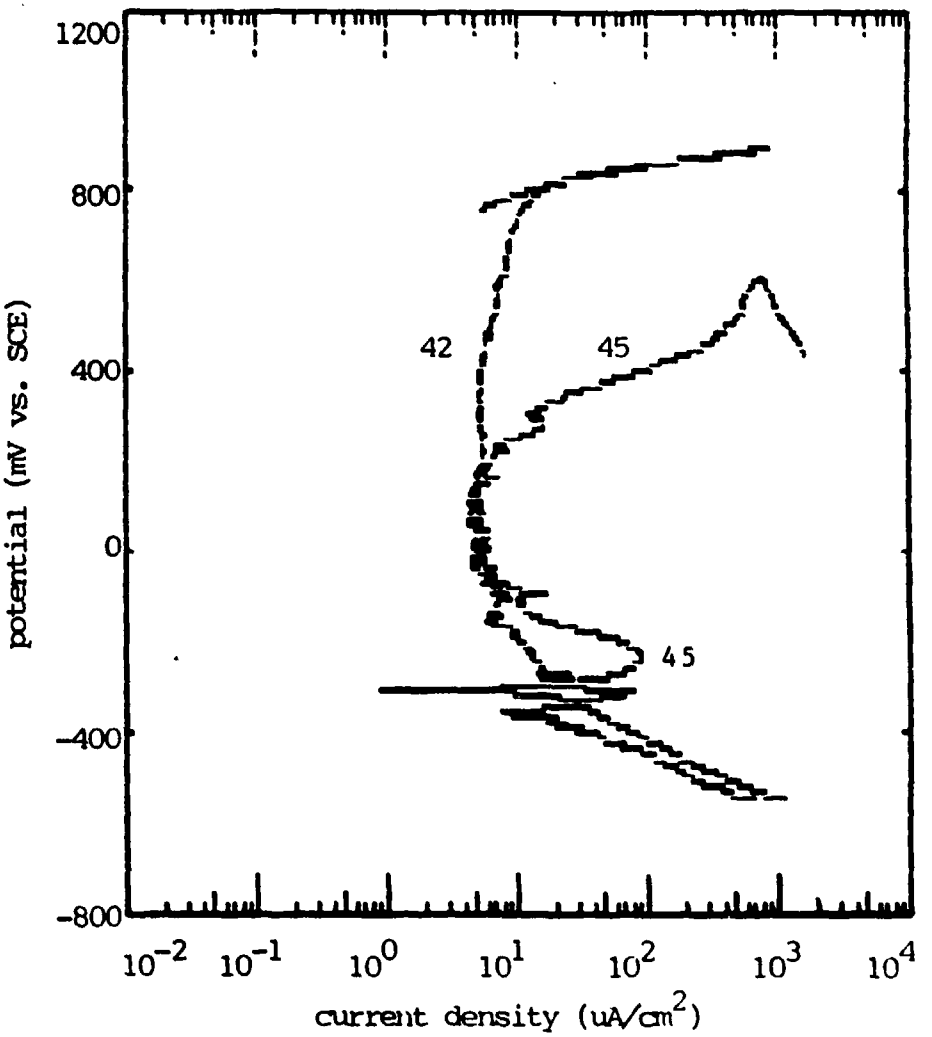

Figure 4: Comparison of the polarization curves of AL6XN ss containing 0.19 wt% N in 2M NaCl + 0.1M HCl at 42 and 45 degrees Celsius.

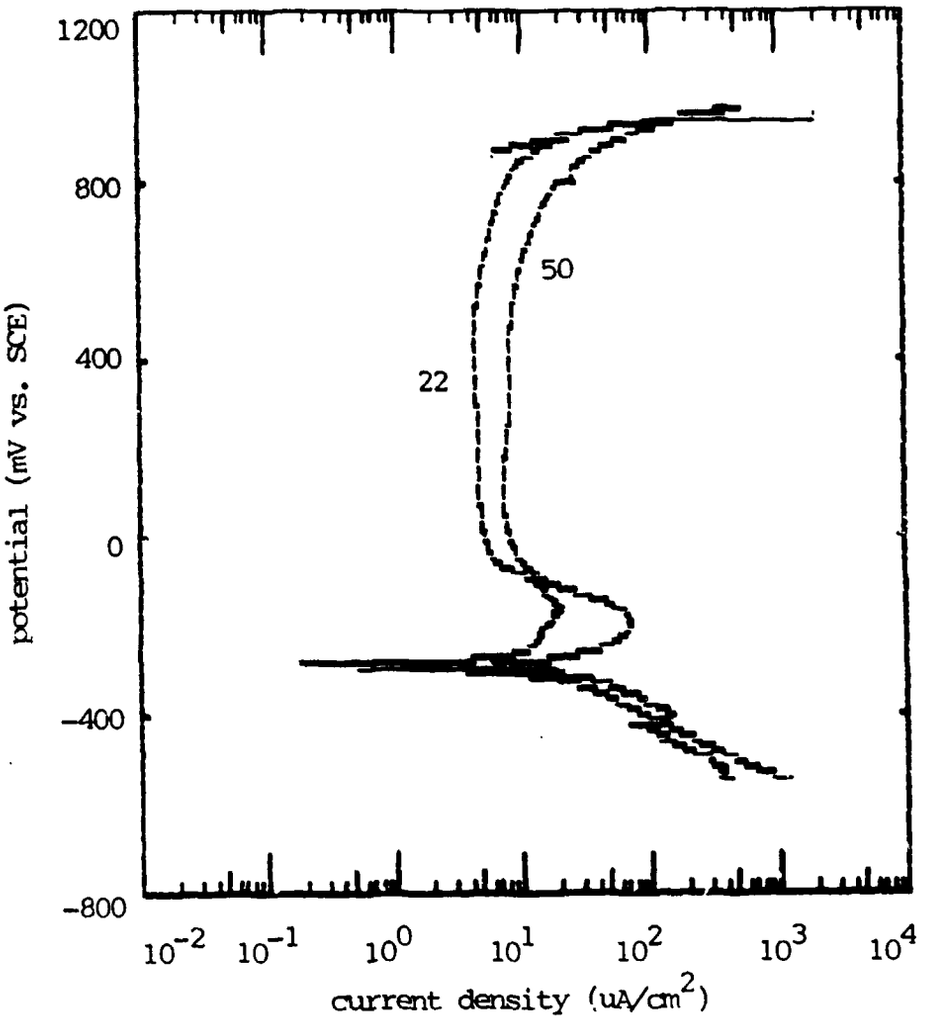

Figure 5: Comparison of the polarization curves of AL6X ss containing 0.04 wt% N in 0.5M H_2SO_4 at 22 and 50 degrees Celsius.

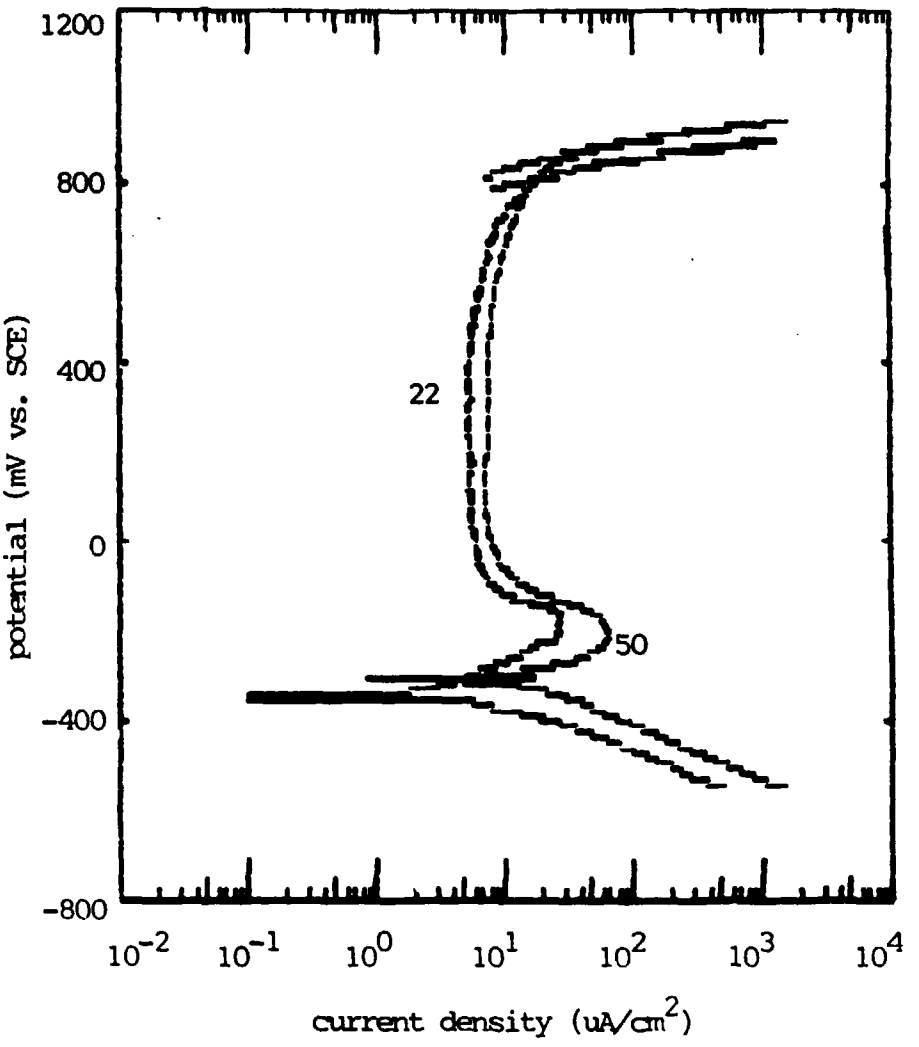

Figure 6: Comparison of the polarization curves of AL6XN ss containing 0.19 wt% N in 0.5M H_2SO_4 at 22 and 50 degrees Celsius.

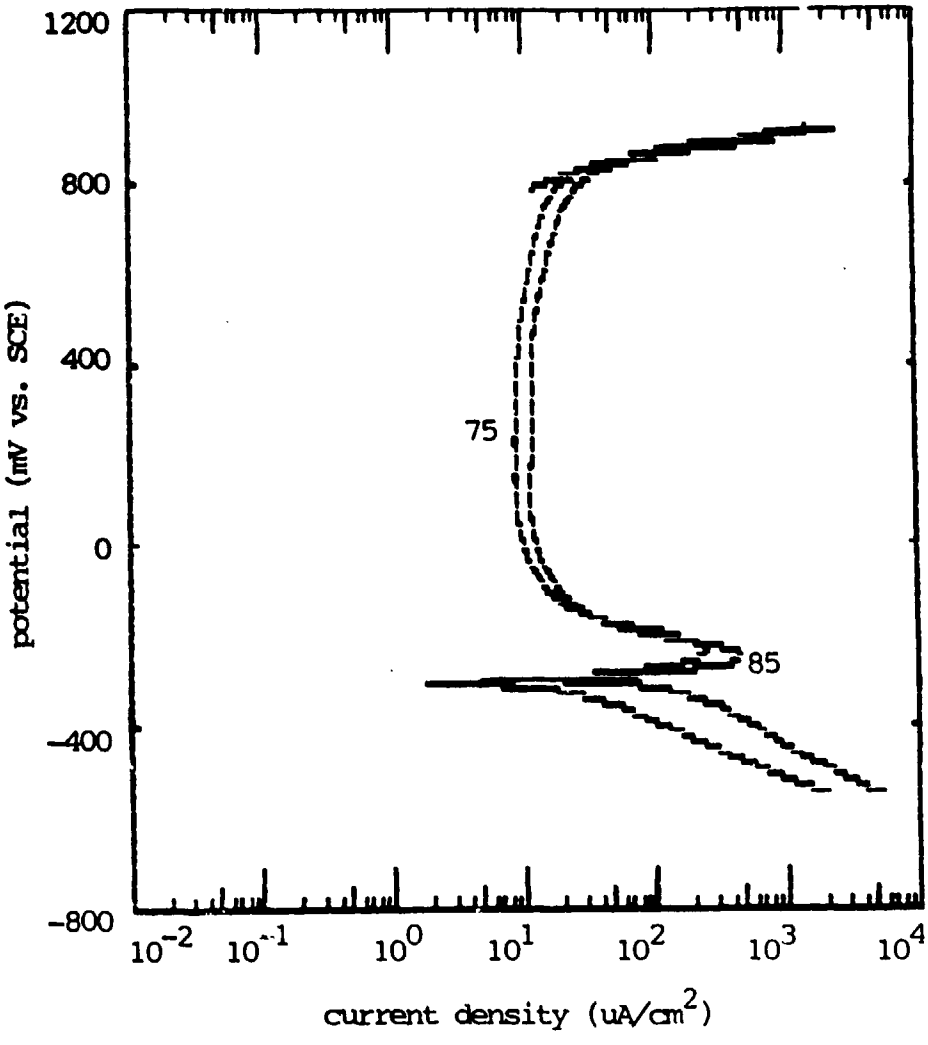

Figure 7: Comparison of the polarization curves of ALCF ss containing 0.04 wt% N in 0.5M H_2SO_4 at 75 and 85 degrees Celsius.

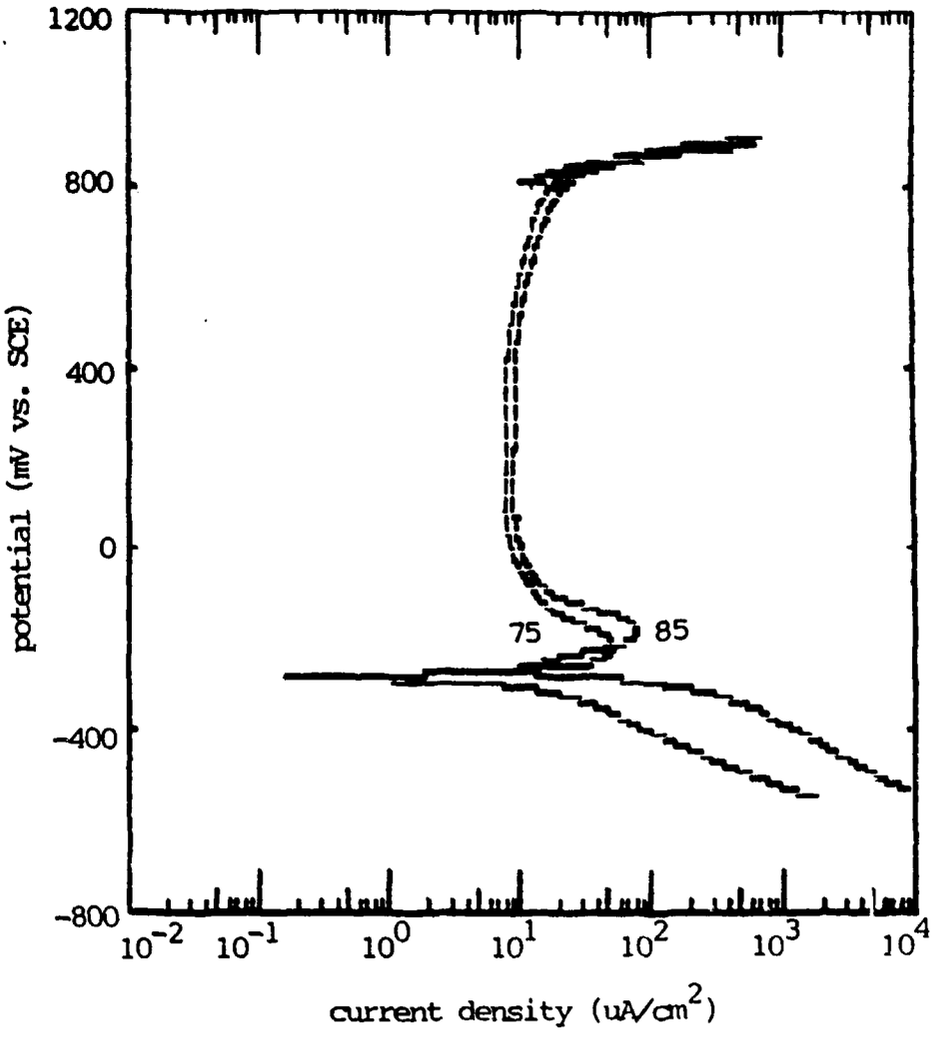

Figure 8: Comparison of the polarization curves of AL6XN ss containing 0.19 wt% N in 0.5M H_2SO_4 at 75 and 85 degrees Celsius.

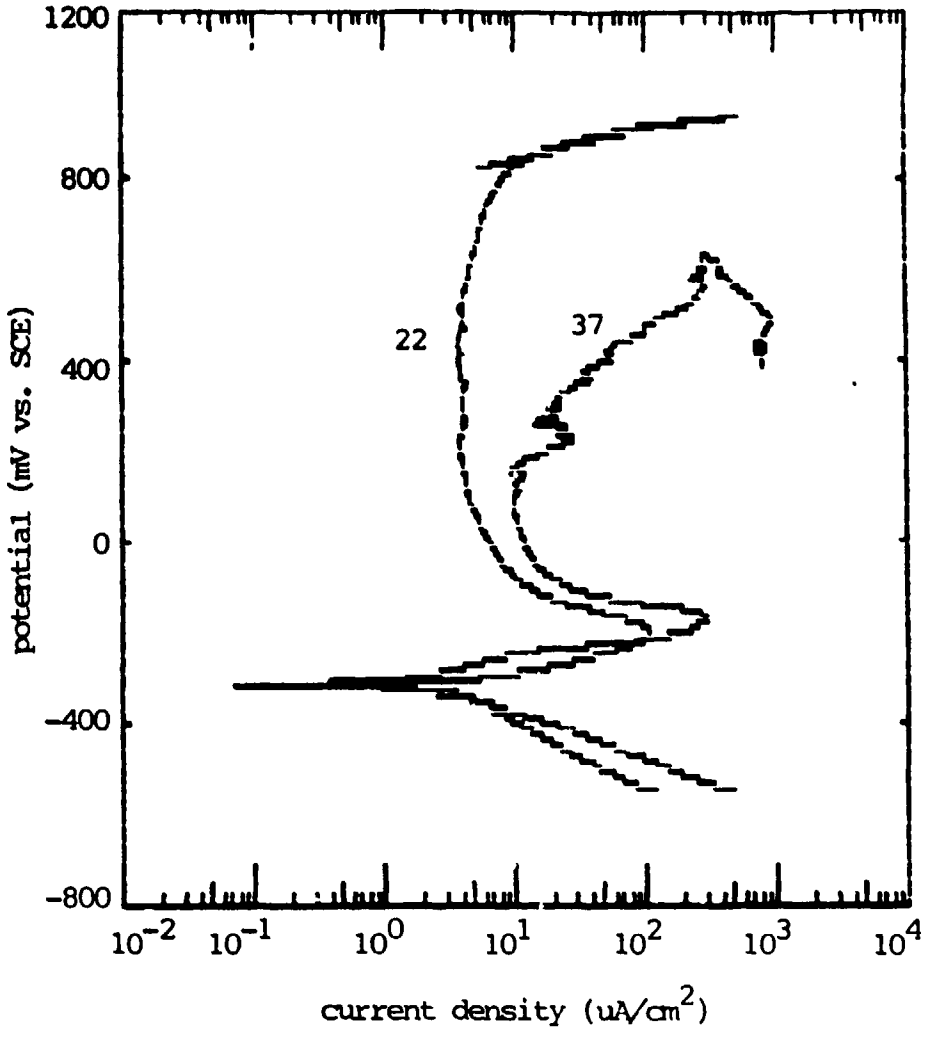

Figure 9: Comparison of the polarization curves of 904L ss containing 0.05 wt% N in 2M NaCl + 0.1M HCl at 22 and 37 degrees Celsius.

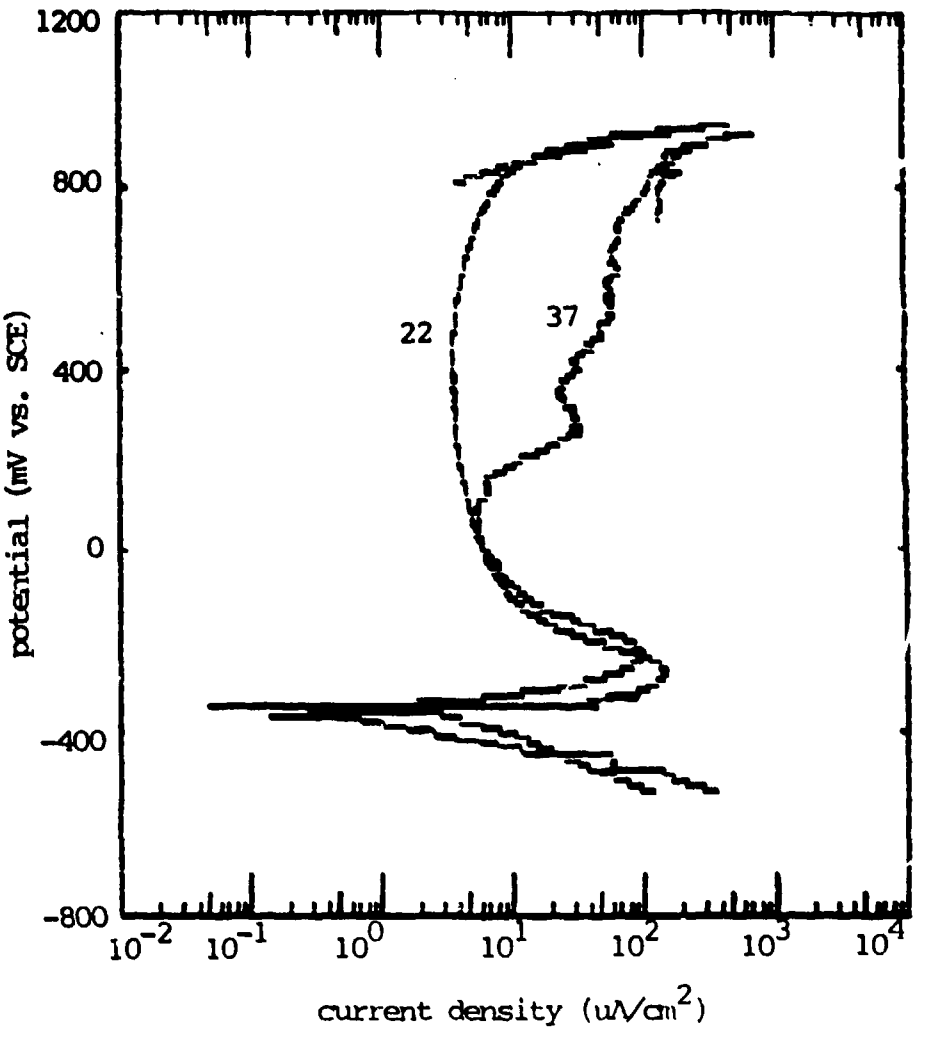

Figure 10: Comparison of the polarization curves of 904LN ss containing 0.20 wt% N in 2M NaCl + 0.1M HCl at 22 and 37 degrees Celsius.

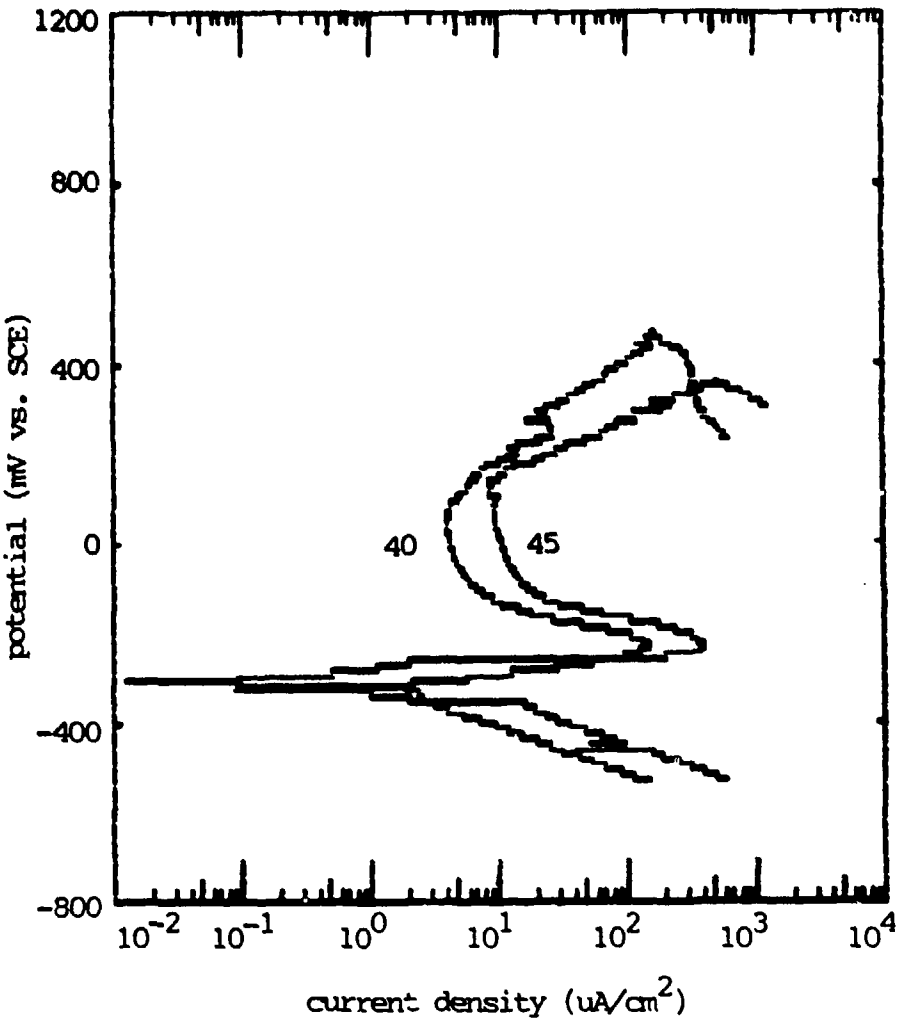

Figure 11: Comparison of the polarization curves of 904L ss containing 0.05 wt% N in 2M NaCl + 0.1M HCl at 40 and 45 degrees Celsius.

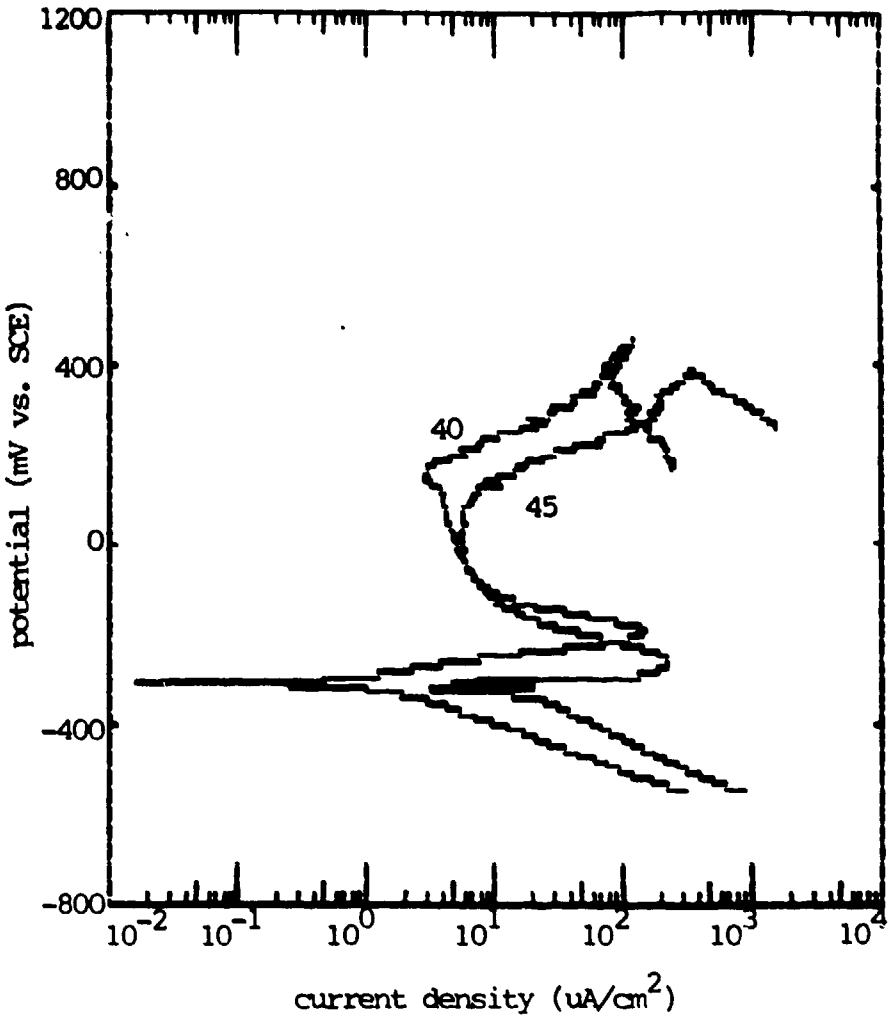

Figure 12: Comparison of the polarization curves of 904IN ss containing 0.20 wt% N in 2M NaCl + 0.1M HCl at 40 and 45 degrees Celsius.